J_ID: Customer A_ID: NSAG040 Copyedited by: Manuscript Category: Original Research Cadmus Art: OP-SOCA2E

Author Query Form

Journal: *Social Cognitive and Affective Neuroscience*
Article Doi: 10.1093/scan/nsag040
Article Title: Fear, anxiety, and the extended amygdala—absence of evidence for strict functional segregation
First Author: Paige R. Didier
Corr. Author: Alexander J. Shackman

AUTHOR QUERIES – TO BE ANSWERED BY THE CORRESPONDING AUTHOR

These proofs are for checking purposes only. They are not in final publication format. Please do not distribute them in print or online. Do not publish this article, or any excerpts from it, anywhere else until the final version has been published with OUP. For further information, see https://academic.oup.com/journals/pages/authors

Figure resolution may be reduced in PDF proofs and in the online PDF, to manage the size of the file. Full-resolution figures will be used for print publication.

Select each question and describe any changes we should make on the proof. Changes against journal style will not be made and proofs will not be sent back for further editing.

AQ1: As per journal style, affiliation IDs should be in numerically sequential order in the author byline. Therefore, we have renumbered the IDs in both the author byline and affiliations. Please carefully review the changes and make any amends directly in the text.

AQ2: Please check the spelling and accuracy of all author names and affiliations, particularly for any co-authors. Also check that author surnames are correctly highlighted. This is to ensure that forenames and surnames are tagged correctly for online indexing. Incorrect names and affiliations may lead to an author not being credited for their work by funders, institutions, or other third parties. Make any changes directly in the text. Note that changes to your authorship list (adding or removing authors, changing designation of corresponding author) require additional approvals. Email journals.corrections@oup.com if this is required.

AQ3: Please note that any email and address details visible on this proof will be published. If you do not have an institutional email or address, and a personal email/home address has been included on these proofs, please indicate if you would prefer for these to be removed. In such cases we will publish the city and country in place of a full address.

AQ4: Please provide University/institution for affiliation 2 directly in the text.

AQ5: Please provide University/institution for affiliation 7 directly in the text.

AQ6: Please provide the complete details [department, university, postal address with the road/street name] for the corresponding author directly in the text.

AQ7: Note that both expansion and abbreviation are provided as keywords “bed nucleus of the stria terminalis (BST/BNST), extended amygdala (EA), Research Domain Criteria (RDoC)”. Please check and make necessary changes if any directly in the text.

AQ8: Please check the heading hierarchy and make any changes directly in the text.

AQ9: As per journal style, section heads have specific wording and appear in a specific order: Introduction, Materials and methods, Results, Discussion, Conclusion. Please check and make necessary changes directly in the text.

AQ10: We have received the following files for publication as supplementary material. didier_shackman_PaxSaxMega_SCAN-25-367R1_Suppl_040826.docx These will be published in the format provided, without edits. If any files need to be removed from this list, specify by responding to this query, stating the filename. If any files need to be added, upload them directly or email them with your proof corrections. If any files need to be updated, upload them directly or email them, without altering the filename. We will seek editor approval for any changes to supplementary material which may delay publication of your article.

AQ11: Please check that funding is recorded in a separate funding section, if applicable. Use the full official names of any funding bodies and include any grant numbers. Insert any changes to the funding section directly in the text.

AQ12: Please note that the reference (Poldrack et al. 2017) is not mentioned (cited) in the text. Add it to the text or delete it from the reference list by making changes directly in the text or references.

AQ13: Please provide the publisher location for reference APA 2022 directly in the reference.

AQ14: Please provide the publisher location for reference Cohen 1988 directly in the reference.

AQ15: Please provide alt text for Figure 1, directly in the text. 'Alt text' is used by screen reading software to describe images to visually impaired readers. Guidance on creating alt text can be found at the following location: link. If you do not provide alt text, we will use the following standard alt text: *For image description, please refer to the figure legend and surrounding text.*

AQ16: Please provide alt text for Figure 2 directly in the text. 'Alt text' is used by screen reading software to describe images to visually impaired readers. Guidance on creating alt text can be found at the following location: link. If you do not provide alt text we will use the following standard alt text: *For image description, please refer to the figure legend and surrounding text.*

AQ17: The caption for Figure 3 currently contains reference to colour used within the figure. For accessibility purposes reference to colour should be avoided unless essential to the understanding of the content. If the reference to colour is not essential to the understanding of the content please provide updated wording for the figure caption to remove reference to colour.

AQ18: Please provide alt text for Figure 3 directly in the text. 'Alt text' is used by screen reading software to describe images to visually impaired readers. Guidance on creating alt text can be found at the following location: link. If you do not provide alt text we will use the following standard alt text: *For image description, please refer to the figure legend and surrounding text.*

AQ19: If your manuscript has figures or text from other sources, please ensure you have permission from the copyright holder. Also ensure that the copyright owner is properly credited, for instance in the figure legends. Make any changes directly in the text. For any questions about permissions, contact jnls.author.support@oup.com.

AQ20: Please provide alt text for Figure 4 directly in the text. 'Alt text' is used by screen reading software to describe images to visually impaired readers. Guidance on creating alt text can be found at the following location: link. If you do not provide alt text we will use the following standard alt text: *For image description, please refer to the figure legend and surrounding text.*

AQ21: Note that the reference Poldrack et al. 2017 has been repeated twice. Hence one of the references has been deleted. Make changes if any directly in the references.

Social Cognitive and Affective Neuroscience, 2026, nsag040
https://doi.org/10.1093/scan/nsag040
Advance Access Publication Date: 3 June 2026
Original Research | Neuroscience

OXFORD

Fear, anxiety, and the extended amygdala—absence of evidence for strict functional segregation

Paige R. Didier[1], Shannon E. Grogans[1], Claire M. Kaplan[2], Hyung Cho Kim[3,4], Samiha Islam[5], Allegra S. Anderson[6], Rachael M. Tillman[7], Manuel Kuhn[8], Juyoen Hur[9], Andrew S. Fox[10,11], Kathryn A. DeYoung[1], Jason F. Smith[1], Alexander J. Shackman[1,3,4,*]

[1]Department of Psychology, University of Maryland, College Park, MD 20742, United States
[2]CommonSpirit Neuropsychology, Lakewood, CO 80228, United States
[3]Neuroscience and Cognitive Science Program, University of Maryland, College Park, MD 20742, United States
[4]Maryland Neuroimaging Center, University of Maryland, College Park, MD 20742, United States
[5]Rees-Jones Center for Foster Care Excellence, Children's Heath, Dallas, TX 75207, United States
[6]Department of Psychiatry and Human Behavior, Brown University, Providence, RI 02912, United States
[7]McGill Neuropsychology, Bethesda, MD 20814, United States
[8]Institute of Medical Psychology, Charité Universitätsmedizin Berlin, Berlin, 10117, Germany
[9]Department of Psychology, Yonsei University, Seoul, 03722, Republic of Korea
[10]Department of Psychology, University of California, Davis, CA 95616, United States
[11]California National Primate Research Center, University of California, Davis, CA 95616, United States

*Corresponding author. E-mail: shackman@umd.edu.

Abstract

Since the time of Freud, the distinction between fear and anxiety has been a hallmark of influential models of emotion and emotional illness, including the Diagnostic and Statistical Manual of Mental Disorders and Research Domain Criteria. Fear and anxiety disorders are common, debilitating, and challenging to treat, underscoring the importance of developing accurate models of the underlying neurobiology. Although there is consensus that the extended amygdala (EA) plays a central role in orchestrating responses to threat, the respective contributions of its two major subdivisions—the central nucleus of the amygdala (Ce) and bed nucleus of the stria terminalis (BST)—remain contentious. To help adjudicate this debate, we performed a harmonized mega-analysis of fMRI data acquired from 295 adults as they completed a well-established threat-anticipation paradigm. Contrary to popular double-dissociation models, results demonstrated that the Ce responds to temporally uncertain threat and the BST responds to certain threat. In direct comparisons, the two regions showed statistically indistinguishable responses, with strong Bayesian evidence of regional equivalence. In contrast, frontocortical regions responded preferentially to uncertain-threat anticipation. Together, these observations underscore the need to reformulate conceptual models that posit a strict segregation of temporally certain and uncertain threat processing in the EA.

Keywords **affective neuroscience, fear and anxiety, bed nucleus of the stria terminalis (BST/BNST), extended amygdala (EA), Research Domain Criteria (RDoC)**

Introduction

Since the time of Freud, the distinction between fear and anxiety has been a hallmark of influential models of emotion and emotional illness, including the DSM and Research Domain Criteria (RDoC) (Freud *et al.* 1959, NIMH 2011, Grupe and Nitschke 2013, Tovote *et al.* 2015, LeDoux and Pine 2016, APA 2022, Grogans *et al.* 2023). When extreme or pervasive, fear and anxiety can become debilitating (Salomon *et al.* 2015). Anxiety disorders are a leading cause of human misery, morbidity, and premature mortality (GBD2021 2024). Existing treatments are far from curative for many, underscoring the need to develop a more complete and accurate understanding of the underlying neurobiology (Singewald *et al.* 2023, Cuijpers *et al.* 2024, De Crescenzo *et al.* 2024).

Received: 15 October 2025. **Revised:** 10 April 2026. **Accepted:** 30 May 2026

There is widespread consensus that the extended amygdala (EA)—a macrocircuit encompassing the central nucleus of the amygdala (Ce) and bed nucleus of the stria terminalis (BST)—plays a central role in fear and anxiety-related states, traits, and disorders, but the precise contributions of the Ce and BST remain contentious (Hur *et al.* 2020, Daniel-Watanabe and Fletcher 2022, Blanchard and Canteras 2024, Shackman *et al.* 2024). Building on an earlier generation of rodent studies (Shackman and Fox 2016), RDoC and other double-dissociation models organize fear and anxiety into two strictly segregated neural systems [Figure S1 (see online supplementary material for a color version of this figure) and Note 1]: the *Acute Threat* system is centered on the amygdala (including the Ce), is sensitive to certain (but not uncertain) threat, and promotes signs and symptoms of fear, whereas the *Potential Threat* system is centered on the BST, is sensitive to uncertain (but not certain) threat, and promotes anxiety (NIMH 2011, Avery *et al.* 2016, LeDoux and Pine 2016). Yet a growing body of rodent mechanistic data casts doubt on this strict either/or perspective (Gungor and Paré 2016, Marcinkiewcz *et al.* 2016, Lange *et al.* 2017, Lee *et al.* 2017, Ahrens *et al.* 2018, Pomrenze *et al.* 2019a, 2019b, Ressler *et al.* 2020, Bruzsik *et al.* 2021, Griessner *et al.* 2021, Marvar *et al.* 2021, Chen *et al.* 2022, Holley and Fox 2022, Moscarello and Penzo 2022, Ren *et al.* 2022, Zhu *et al.* 2024), motivating the competing hypothesis that the Ce and BST play a role in organizing responses to both kinds of threat (Gungor and Paré 2016, Fox and Shackman 2019, Daniel-Watanabe and Fletcher 2022).

To help adjudicate this debate, we performed a harmonized mega-analysis of fMRI data acquired from 295 racially diverse adults as they completed the Maryland Threat Countdown (MTC), a well-established threat-anticipation paradigm (Fig. 1) (Hur *et al.* 2020). The MTC is an fMRI-optimized variant of temporally certain/uncertain-threat assays that have been behaviorally and pharmacologically validated in rodents and humans, maximizing translational relevance (Hur *et al.* 2020). Data were acquired using a multiband sequence and re-processed using a singular best-practices pipeline. The relatively large sample afforded the power necessary to reliably detect small differences in regional responses to certain- and uncertain-threat anticipation ($d \geq 0.16$).

Because voxelwise analyses do not permit inferences about regional differences, we used *a priori* anatomical regions of interest (ROIs) to rigorously compare the Ce and BST. This has the advantage of providing statistically unbiased effect-size estimates (Poldrack *et al.* 2017), in contrast to earlier work by our group that relied on functionally defined ROIs (Hur *et al.* 2020). To maximize anatomical resolution and inferential clarity, mean activation was computed using spatially unsmoothed data. Hypothesis testing focused on regional responses to certain- and uncertain-threat anticipation relative to their perceptually similar reference conditions (e.g. certain-safety anticipation), providing sharper inferences than prior work focused on baseline contrasts (Grogans *et al.* 2024). Of course, traditional null-hypothesis tests cannot address whether the Ce and BST show statistically equivalent responses to certain- and uncertain-threat anticipation. Here, we used a Bayesian framework to quantify the strength of the evidence for and against regional differences. The Bayesian approach provides well-established benchmarks for interpreting effect sizes and sidesteps the need to arbitrarily choose what constitutes a "statistically indistinguishable" difference (Bo *et al.* 2024), unlike work focused on frequentist equivalence tests (Shackman *et al.* 2024). Whole-brain voxelwise analyses enabled us to explore less intensively scrutinized regions.

Method

Overview of the mega-analysis

The neuroimaging mega-analysis capitalized on data from two previously published fMRI studies focused on the neural circuits recruited by temporally certain- and uncertain-threat anticipation. The first study encompassed a sample of 220 psychiatrically healthy, first-year university students (Grogans *et al.* 2024). The second encompassed 75 tobacco smokers recruited from the surrounding community (Kim *et al.* 2023). Both studies employed the same certain/uncertain threat-anticipation paradigm (Maryland Threat Countdown task) and were collected using identical parameters on the same scanner using the same head-coil. For the mega-analysis, all neuroimaging data were completely reprocessed using a singular best-practices pipeline, as detailed below. This harmonized approach is increasingly common and generally provides greater statistical power and generalizability, relative to typical single-study approaches (Petre *et al.* 2022, Radua *et al.* 2025), and greater anatomical resolution and statistical rigor, as compared to coordinate-based meta-analytic approaches (Costafreda 2009, Salimi-Khorshidi *et al.* 2009). All participants provided informed written consent. Procedures were approved by the University of Maryland, College Park Institutional Review Board (protocols #659385 and #824438).

Detailed descriptions of the study designs, enrollment criteria, participants, data collection procedures, and data exclusions are provided in the original reports (Kim *et al.* 2023, Grogans *et al.* 2024). The mega-analysis was not pre-registered.

Participants

Across studies, a racially diverse sample of 295 participants provided usable neuroimaging data (Total: 45.4% female; 52.2% White Non-Hispanic, 16.6% Asian, 19.0% African American, 4.1% Hispanic, 8.1% Multiracial/Other; $M = 21.6$ years, SD = 5.7, range = 18–40 years; University Students: 49.5% female; 61.4% White Non-Hispanic, 18.2% Asian, 8.6% African American, 4.1% Hispanic, 7.3% Multiracial/Other; $M = 18.8$ years; SD = 0.4; Community Tobacco Smokers: 33.3% female; 25.3% White Non-Hispanic, 12.0% Asian, 49.3% African American, 4.0% Hispanic, 9.4% Multiracial/Other; $M = 30.1$ years; SD = 5.6). Of these, eight participants were excluded from skin conductance analyses due to insufficient usable data (for additional details regarding data censoring, see Grogans *et al.* 2024 and Kim *et al.* 2023).

Power analysis

To enable readers to better interpret in our results, we performed a post hoc power analysis. G-power (version 3.1.9.2) indicated that the final sample of 295 usable fMRI datasets provides 80% power to detect "small" mean differences in regional activation (Cohen's $d = 0.16$, $\alpha = 0.05$, two-tailed; Cohen 1988, Faul *et al.* 2007).

Threat-anticipation paradigm

As shown in Fig. 1, the Maryland Threat Countdown paradigm takes the form of a 2 (*Valence:* Threat/Safety) × 2 (*Temporal Certainty:* Uncertain/Certain) design. On Certain-Threat trials, participants saw a descending stream of integers ("count-down") for 18.75 s. To ensure robust emotion, the anticipation epoch culminated with the presentation of a noxious electric shock, unpleasant photograph, and

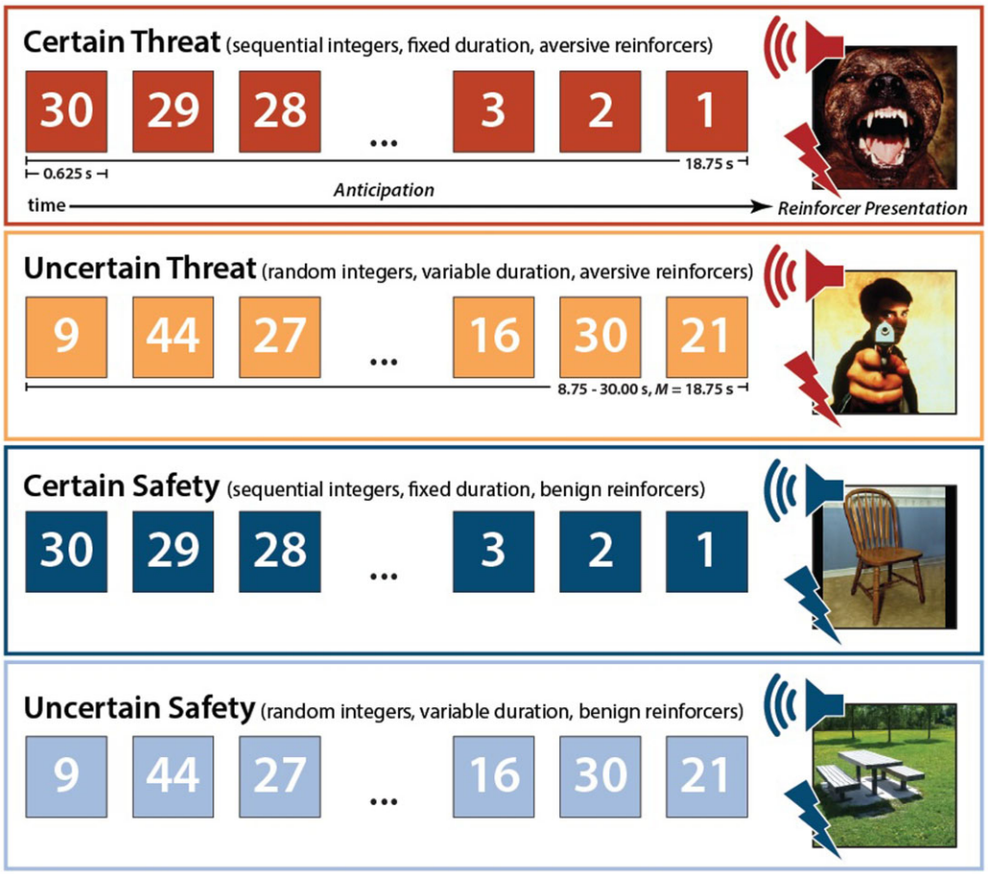

Figure 1 Maryland threat countdown fMRI paradigm. The paradigm takes the form of a 2 (*Valence*: Threat, Safety) × 2 (*Temporal Certainty*: Certain, Uncertain) randomized event-related design. Participants were completely informed about the task design and contingencies prior to scanning. On certain-threat trials, participants saw a descending stream of integers ("countdown") for 18.75 s. To ensure robust distress and arousal, the anticipation epoch always terminated with the presentation of a noxious electric shock, unpleasant photograph, and thematically related audio clip (e.g. scream). Uncertain-threat trials were similar, but the integer stream was randomized and presented for an uncertain and variable duration (8.75–30.00 s; $M = 18.75$ s). Participants knew that something aversive was going to occur, but they had no way of knowing precisely *when*. Safety trials were similar but terminated with the delivery of emotionally neutral reinforcers (e.g. just-perceptible electrical stimulation).

thematically related audio clip. Uncertain-Threat trials were similar, but the integer stream was randomized and presented for an uncertain and variable duration (8.75-30.00 s; $M = 18.75$ s). Participants knew that something aversive was going to occur but had no way of knowing precisely when. The Maryland paradigm differs from threat-anticipation tasks (e.g. NPU) that manipulate the probability (or probability *and* timing) of encounters (Schmitz and Grillon 2012). For additional details, see the Supplementary Material. Participants were periodically prompted to rate the intensity of fear/anxiety experienced a few seconds earlier, during the anticipation period of the prior trial, using a 1 (minimal) to 4 (maximal) scale. Skin conductance was continuously acquired throughout (for details, see the Supplementary Material).

MRI data acquisition

Data were acquired using a Siemens Magnetom TIM Trio 3 Tesla scanner (32-channel head-coil; for additional details, see the Supplementary Material). T1-weighted anatomical images were acquired using a magnetization prepared rapid acquisition gradient echo sequence (TR = 2400 ms; TE = 2.01 ms; inversion time = 1060 ms; flip = 8°; slice thickness = 0.8 mm; in-plane = 0.8 × 0.8 mm; matrix = 300 × 320; field-of-view = 240 × 256). A T2-weighted image was collected co-planar to the T1-weighted image (TR = 3200 ms; TE = 564 ms; flip angle = 120°). A multi-band sequence was used to collect oblique-axial echo-planar imaging (EPI) volumes (acceleration = 6; TR = 1250 ms; TE = 39.4 ms; flip = 36.4°; slice thickness = 2.2 mm, slices = 60; in-plane =2.1875 × 2.1875 mm; matrix = 96 × 96; 3 × 478-volume scans). Co-planar oblique-axial spin echo (SE) images were collected in opposing phase-encoding directions (rostral-to-caudal and caudal-to-rostral; TR = 7220 ms; TE = 73 ms). Respiration and pulse were continuously acquired.

MRI pipeline

Methods are similar to other work and are only briefly summarized here (Cornwell *et al.* 2025). For details, see the Supplementary Material.

Anatomical data processing

T1- and T2-weighted images were inhomogeneity corrected, denoised, and brain-extracted. Extracted T1 images were

diffeomorphically normalized to a 1-mm T1-weighted MNI152 template using *ANTS*.

Functional data processing

EPI files were de-spiked, slice-time corrected, motion-corrected, inhomogeneity corrected, co-registered using boundary-based registration, normalized to the MNI template, and resampled (2 mm^3). Voxelwise analyses employed data that were spatially smoothed (4 mm). Extended amygdala (EA) analyses used spatially unsmoothed data and anatomical regions-of-interest (ROIs; see below).

fMRI data modeling

Methods are similar to other recent work and only briefly summarized here (Cornwell *et al.* 2025). For additional details, see the Supplementary Material.

First-level modeling

Modeling was performed using *SPM12*, the default autoregressive model, and a temporal band-pass filter set to the hemodynamic response function (HRF) and 128 s set to the hemodynamic response function (HRF) and 128 s (0.0078-0.1667 Hz). Regressors were convolved with a canonical HRF and temporal derivative. For the threat-anticipation paradigm, hemodynamic activity was modeled using rectangular regressors spanning the entirety of the anticipation ("countdown") epochs of the Uncertain-Threat, Certain-Threat, and Uncertain-Safety trials. Certain-Safety anticipation served as the reference condition and contributed to the implicit baseline estimate. Epochs corresponding to the reinforcers, visual masks, and rating prompts were modeled using the same approach. Nuisance variates included volume-to-volume displacement and first derivative, six motion parameters and first derivatives, cerebrospinal fluid (CSF), pulse, respiration, and other nuisance signals (e.g. brain edge, CSF edge, global motion, WM, and extracerebral soft tissue). Volumes with excessive displacement (>0.5 mm) and those during and immediately following reinforcer (shock) delivery were censored.

ROIs

Ce and BST activation was quantified using anatomical ROIs, unsmoothed data, and regression coefficients extracted and averaged for each combination of contrast, region, and participant (Theiss *et al.* 2017, Tillman *et al.* 2018). Anatomical ROIs enable statistically unbiased tests of regional sensitivity to specific experimental manipulations (i.e. Region × Condition effects), including potential single and double dissociations (e.g. BST: Uncertain > Certain Threat; Ce: Uncertain < Certain Threat) (Poldrack *et al.* 2017, Fox *et al.* 2018). ROI registration appeared reasonable for both regions and hemispheres, based on visual inspection of the 295 normalized T1-weighted anatomical images.

Analytic strategy

Methods are similar to other work and are only briefly summarized here (Cornwell *et al.* 2025). For details, see the Supplementary Material.

Overview

Frequentist (Cohen's *d*) effect sizes were interpreted using established benchmarks (Cohen 1988, 1994, Schimmack 2019), ranging from *large* ($d = 0.80$), to *medium* ($d = 0.50$), to *small* ($d = 0.20$), to *nil* ($d \leq 0.10$). Bayesian effect sizes were computed for select analyses. Bayes factor (BF_{10}) quantifies the relative performance of the null hypothesis (H_0; e.g. the absence of a credible mean difference) and the alternative hypothesis (H_1; e.g. the presence of a credible mean difference), on a 0 to ∞ scale. BF can be used to quantify the relative strength of the evidence for H_0 (test the null), unlike conventional frequentist null-hypothesis significance tests (Wagenmakers *et al.* 2018, Bo *et al.* 2024). It also does not require the data analyst to arbitrarily decide what constitutes a "statistically indistinguishable" difference, in contrast to traditional equivalence tests (Hur *et al.* 2020). This approach provides readily interpretable, principled effect-size benchmarks (van Doorn *et al.* 2021). Values >1 were interpreted as evidence of mean differences in activation across conditions, ranging from *strong* ($BF_{10} > 10$), to *moderate* (BF_{10} = 3–10), to *weak* (BF_{10} = 1–3). Values <1 were interpreted as evidence of statistical equivalence (i.e. support for the null hypothesis), ranging from *strong* ($BF_{10} < 0.10$), to *moderate* (BF_{10} = 0.10–0.33), to *weak* (BF_{10} = 0.33–1). The reciprocal of BF_{10} represents the relative likelihood of the null hypothesis (e.g. BF_{10}=0.10, H_0 is 10 times more likely than H_1). Bayesian effects were computed using a noninformative zero-centered Cauchy distribution ($\omega = 1/\sqrt{2}$), the field standard for two-sided tests (Schönbrodt *et al.* 2017, Wagenmakers *et al.* 2018, Gronau *et al.* 2020, van Doorn *et al.* 2021, Schmalz *et al.* 2023). Across tests, the estimated error of the MCMC-derived (Markov Chain Monte Carlo) BF_{10} estimates was negligible (<0.30%) and stable across a range of priors.

Whole-brain voxelwise tests

Whole-brain voxelwise repeated-measures GLMs were used to compare each threat-anticipation condition to its corresponding control condition (e.g. Uncertain-Threat vs. Uncertain-Safety anticipation), while accounting for mean-centered study (Kim *et al.* 2023, Grogans *et al.* 2024), age, and assigned sex. A minimum conjunction was used to identify voxels sensitive to Certain- *and* Uncertain-Threat anticipation (Nichols *et al.* 2005). We also directly compared Certain- to Uncertain- Threat anticipation.

Regions of interest

One-sample Student's *t*-tests was used to confirm that the EA ROIs showed nominally significant recruitment during Certain and Uncertain Threat anticipation ($P < .05$, uncorrected). We used a standard 2 (*Region:* Ce, BST) × 2 (*Threat-Certainty:* Certain, Uncertain) repeated-measures GLM to test regional differences in activation during the anticipation of temporally Certain Threat (relative to Certain Safety) versus Uncertain Threat (relative to Uncertain Safety). Interactions were probed using focal contrasts. Sensitivity analyses confirmed that none of the conclusions materially changed when controlling for study, age, and assigned sex (for details, see the study OSF collection). A sign test (Z_{Sign}) was used to test the proportion of participants showing double dissociations.

Results

Threat anticipation amplifies subjective distress and objective arousal

We used repeated-measures general linear models (GLMs) to confirm that the threat-anticipation paradigm had the intended impact on anticipatory distress (in-scanner ratings) and arousal (skin conductance

level, SCL). Eight participants were excluded from SCL analyses due to insufficient usable data ($n = 287$). As shown in Fig. 2a, subjective feelings of fear and anxiety were significantly elevated during the anticipation of threat compared to safety, and distress was particularly pronounced when the timing of threat encounters was uncertain (*Valence:* $F(1,294) = 965.74$, $P < .001$, $d = 1.81$ [1.62, 1.99], $BF_{10} = 1.42 \times 10^{91}$; *Certainty:* $F(1,294) = 231.95$, $P < .001$, $d = 0.89$ [0.75, 1.02], $BF_{10} = 3.91 \times 10^{35}$; *Valence × Certainty:* $F(1,294) = 25.58$, $P < .001$, $d = 0.29$ [0.18, 0.41], $BF_{10} = 12\,327.09$; *Threat, Uncertain vs. Certain:* $F(1,294) = 154.04$, $P < .001$, $d = 0.72$ [0.59, 0.85], $BF_{10} = 3.14 \times 10^{25}$; *Safety, Uncertain vs. Certain:* $F(1,218) = 77.63$, $P < .001$, $d = 0.51$ [0.39, 0.63], $BF_{10} = 4.42 \times 10^{13}$).

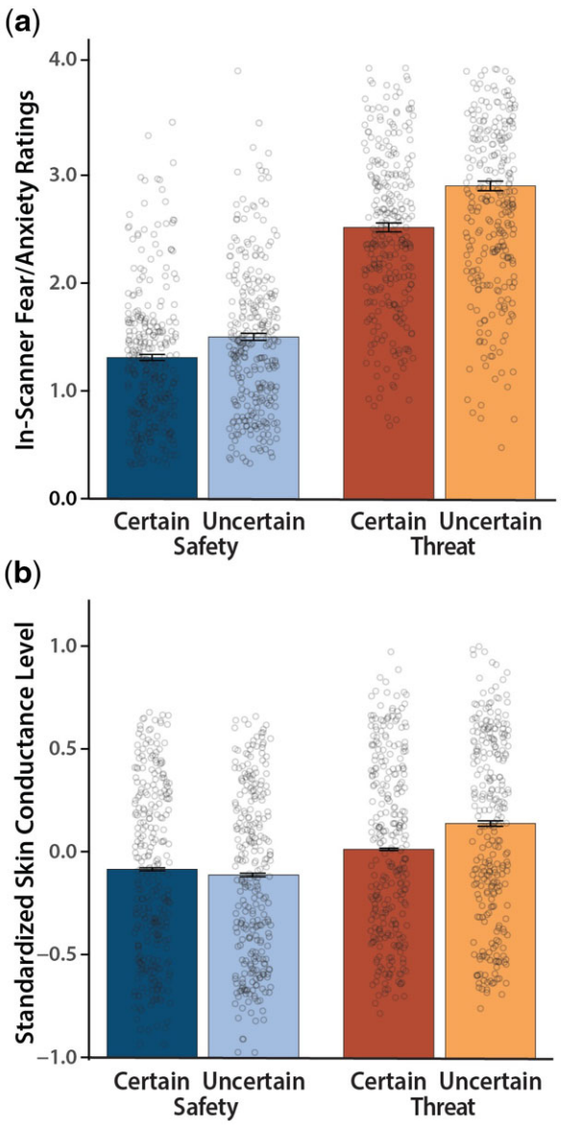

Figure 2 The Maryland Threat Countdown paradigm is a valid probe of human fear and anxiety. (a) Anticipated threat increases subjective symptoms of distress. Conscious feelings of fear and anxiety were increased during the anticipation of threat compared to safety, and this was particularly evident for temporally uncertain threat ($P < .001$). (b) Anticipated threat increases objective signs of arousal. A similar pattern was evident for skin conductance level (SCL; $P < .001$). Bars depict means, whiskers depict standard errors, and open rings depict individual participants.

As shown in Fig. 2b, the same general pattern was evident for SCL, an objective psychophysiological index of anticipatory arousal (*Valence:* $F(1,286) = 165.76$, $P < .001$, $d = 0.76$ [0.63, 0.89], $BF_{10} = 9.61 \times 10^{26}$; *Certainty:* $F(1,286) = 80.21$, $P < .001$, $d = 0.53$ [0.41, 0.65], $BF_{10} = 1.09 \times 10^{14}$; *Valence × Certainty:* $F(1,286) = 129.87$, $P < .001$, $d = 0.67$ [0.54, 0.80], $BF_{10} = 7.53 \times 10^{21}$; *Threat, Uncertain vs. Certain:* $F(1,286) = 120.97$, $P < .001$, $d = 0.65$ [0.52, 0.78], $BF_{10} = 3.49 \times 10^{20}$; *Safety, Uncertain vs. Certain:* $F(1,286) = 43.61$, $P < .001$, $d = -0.39$ [−0.51, −0.27], $BF_{10} = 3.57 \times 10^{7}$). Taken together, these converging observations confirm the validity of the MTC paradigm as an experimental probe of human fear and anxiety, consistent with work in smaller samples (Hur *et al.* 2020, Kim *et al.* 2023).

Uncertain-threat anticipation recruits a distributed cortico-subcortical network

We used a whole-brain voxelwise GLM to identify regions recruited during the anticipation of temporally uncertain threat, relative to uncertain safety ($P < .05$, whole-brain FWE corrected). As shown in the first column of Fig. 3, this revealed a widely distributed network of cortical and subcortical regions previously implicated in the expression and regulation of human fear and anxiety (Chavanne and Robinson 2021, Shackman and Fox 2021, Hur *et al.* 2022, Bo *et al.* 2024, Grogans *et al.* 2024, Radua *et al.* 2025), including the midcingulate cortex (MCC); anterior insula (AI) extending into the frontal operculum (FrO); dorsolateral prefrontal cortex (dlPFC) extending to the frontal pole (FP); brainstem encompassing the periaqueductal grey (PAG); basal forebrain, including the BST; and dorsal amygdala, including the Ce (Table S1, see online supplementary material for a color version of this table).

While not the focus of our study, exploratory analyses indicated that uncertain-threat anticipation was associated with reduced activation ("de-activation") in a set of midline regions that encompassed key nodes of the default mode network (e.g. frontal pole, rostral and straight gyri, and precuneus) as well as the pre- and post-central gyri, posterior insula, parahippocampal gyrus, and hippocampus (Table S2, see online supplementary material for a color version of this table), dovetailing with prior observations (Choi *et al.* 2012, Grupe *et al.* 2016, Hur *et al.* 2020). At a more liberal threshold (FDR $q < 0.05$), the same pattern was evident in ventromedial regions of the amygdala (e.g. basal and cortical nuclei and amygdalohippocampal transition area), consistent with prior neuroimaging studies of anticipated threat and with the known functional heterogeneity of this complex structure (Murty *et al.* 2022, 2023, Fox and Shackman 2024, Cornwell *et al.* 2025).

Certain-threat anticipation recruits a broadly similar network

We used a parallel approach to identify regions recruited during the anticipation of temporally certain threat, relative to certain safety ($P < .05$, whole-brain FWE corrected). As shown in the second column of Fig. 3, the results strongly overlapped those evident for uncertain threat (Tables S3 and S4, see online supplementary material for a color version of these tables). Indeed, a minimum-conjunction analysis of the two contrasts (Logical "AND"; Nichols *et al.* 2005) revealed voxelwise colocalization in every key region, including the BST and dorsal amygdala in the region of the Ce (third column of Fig. 3). Taken

J_ID: Customer A_ID: NSAG040 Copyedited by: Manuscript Category: Original Research Cadmus Art: OP-SOCA26

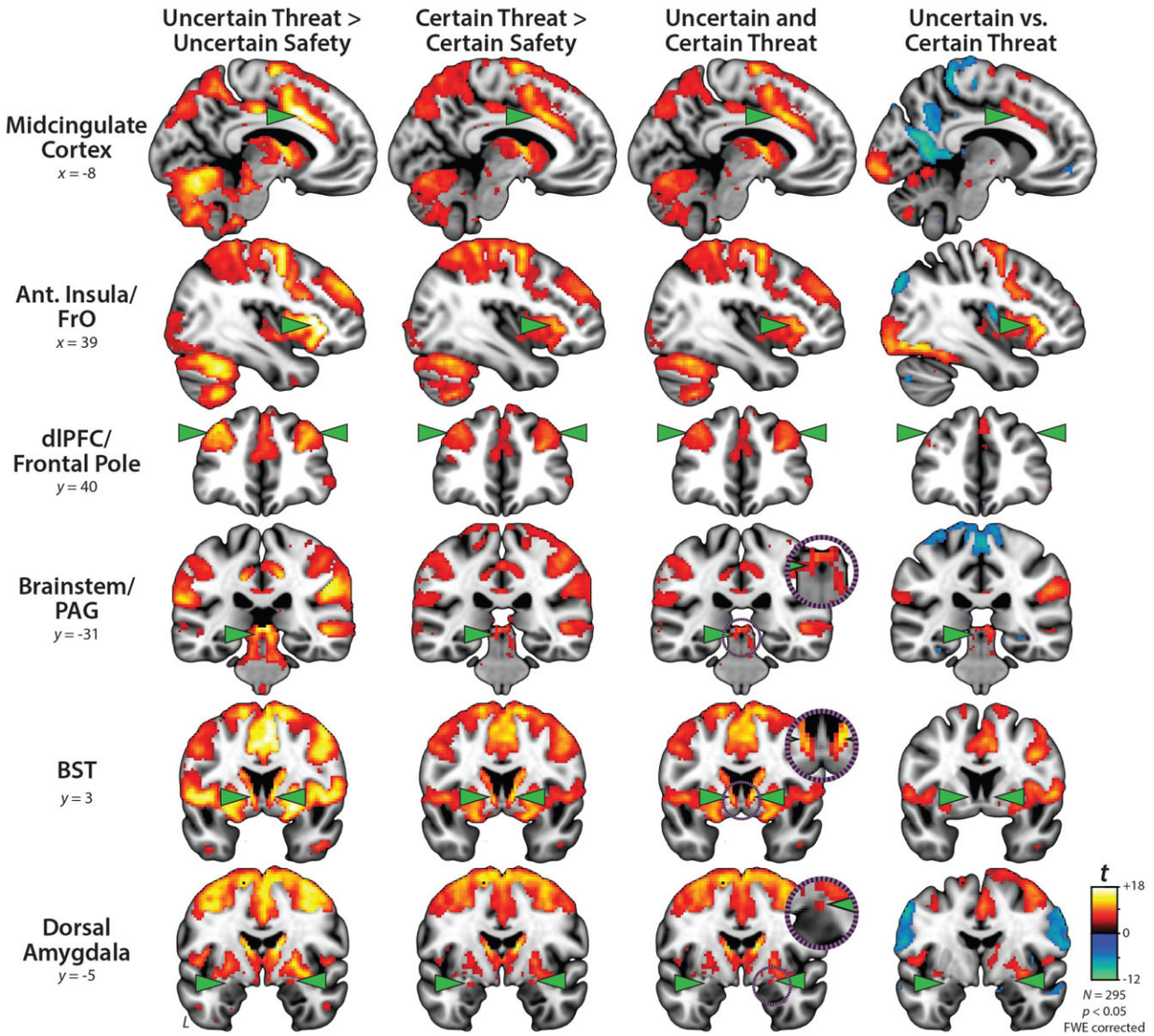

Figure 3 Uncertain- and certain-threat anticipation recruit a common cortico-subcortical network. Key regions (*green arrowheads*) show significantly increased activation during the anticipation of both uncertain threat (*first column*) and certain threat (*second column*), relative to their respective control conditions ($P < .05$, whole-brain FWE corrected). *Third column* depicts the voxelwise conjunction (logical "AND") of the two thresholded contrasts. Co-localization is evident throughout the network, including the BST and dorsal amygdala (Ce). *Fourth column* shows the direct contrast of the two threat-anticipation conditions. The MCC, AI/FrO, and to a lesser extent dlPFC/FP, show significantly greater activation during the anticipation of uncertain threat, whereas the BST, dorsal amygdala (Ce), and PAG show negligible discrimination of the two conditions. The dlPFC/FP mean difference was more evident at more rostral planes. For additional details, see Tables S1–S6 (see online supplementary material for a color version of these tables). *Purple insets* depict magnified views of overlap in the PAG, BST, and Ce. Abbreviations: Ant., anterior; BST, bed nucleus of the stria terminalis; dlPFC, dorsolateral prefrontal cortex; FrO, frontal operculum; FWE, familywise error; PAG, periaqueductal gray.

together, these results suggest that this distributed cortico-subcortical system is sensitive to a range of anticipated threats, including those that are certain and uncertain in their timing.

Frontocortical regions discriminate uncertain from certain threat, subcortical regions do not

To determine whether regions recruited during threat anticipation are sensitive to temporal uncertainty, we directly compared the uncertain and certain threat conditions ($P < .05$, whole-brain FWE corrected). As shown in the fourth column of Fig. 3, frontocortical regions—including MCC, AI/FrO, and dlPFC/FP—while engaged by both kinds of threat, showed a preference for temporally uncertain threat, consistent with prior work (Tables S5 and S6, see online supplementary material for a color version of these tables) (Hur *et al.* 2020). In contrast, the BST, dorsal amygdala (Ce), and PAG showed negligible differences.

The BST and Ce show statistically indistinguishable responses to certain- and uncertain-threat anticipation

Because voxelwise analyses do not permit inferences about regional differences in activation, we used anatomical ROIs and spatially

unsmoothed data to rigorously compare the BST and Ce (Fig. 4a). As a precursor to hypothesis testing, we used one-sample *t*-tests to confirm that the BST and Ce ROIs show significant activation during certain- and uncertain-threat anticipation relative to their respective control conditions ($t(294)>6.49$, $P<.001$, $d>0.37$, $BF_{10}>2.02\times10^{7}$). Next, we used a standard 2 (*Region:* BST, Ce) × 2 (*Threat-Certainty:* Certain, Uncertain) repeated-measures GLM to probe potential regional differences in threat sensitivity. Here again the BST and Ce proved statistically indistinguishable (Fig. 4a, Figure S2A and B, see online supplementary material for a color version of this figure). The critical Region × Threat-Certainty contrast was not significant ($F(1,294)$ = 0.12, P = .73, d = −0.02 [−0.13, 0.09], BF_{10} = 0.07). In fact, participants were just as likely as not (49.5% vs. 50.5%; H_0 = 50.0%) to show the hypothesized double-dissociation pattern (Z_{Sign} = 0.12, P = .91; Fig. 4b, Figure S2C, see online supplementary material for a color version of this figure). Focal contrasts indicated that neither the BST nor the Ce credibly discriminated certain- from uncertain-threat anticipation (*BST:* $t(294)$ = −0.59, P = .56, d = −0.03 [−0.15, 0.08], BF_{10} = 0.11; *Ce:* $t(294)$ = −1.38, P = .17, d = −0.08 [−0.19, 0.03], BF_{10} = 0.03; Fig. 4a), consistent with the more conservatively thresholded voxelwise results (Fig. 3). The GLM did, however, reveal a main effect of region, reflecting generally greater BST reactivity to both kinds of anticipated threat ($F(1,294)$ = 95.36, $P<.001$, d = 0.57 [0.45, 0.69], $BF_{10}=3.95\times10^{16}$). The main effect of Threat-Certainty was not significant (P = .22, d = −0.07 [−0.19, 0.04], BF_{10} = 0.14). None of the conclusions materially changed when mean-centered study, age, and biological sex were included as nuisance variates. In sum, at least when viewed through the lens of hemodynamics and the MTC paradigm, the BST and Ce show statistically indistinguishable responses to certain- and uncertain-threat anticipation.

Discussion

In the realm of human neuroimaging research, the present results provide some of the strongest evidence to date that the functional architecture of the EA does not conform to popular double-dissociation models (Figure S1, see online supplementary material for a color version of this figure and Note 1; NIMH 2011, Somerville *et al.* 2013, Avery *et al.* 2016, LeDoux and Pine 2016, Klumpers *et al.* 2017). The Ce and BST are both engaged during periods of threat anticipation, and the degree of engagement is independent of the temporal certainty of threat encounters. In a head-to-head comparison, the Ce and BST showed statistically indistinguishable selectivity for the two kinds of threat (d = 0.02), with strong Bayesian evidence against regional differences (BF_{10} = 0.07; H_0 is 14.3 times more likely than H_1).

It is worth considering two potential methodological explanations for this null observation. First, might it reflect inadequate EA signal quality (e.g. low signal-to-noise ratio [SNR])? This is unlikely. Our results indicate that we have sufficient statistical power and SNR to detect threat-related activation in the Ce and BST and to detect other types of regional activation differences (i.e. greater BST sensitivity to anticipated threat). Second, might it reflect an artifact of our hemodynamic model? After all, our conclusions are based on a simplified "boxcar" model that assumes static, time-invariant neural responses to anticipated threats. This approach precludes inferences about regional differences in more fleeting activation dynamics, and leaves open the possibility that the Ce and BST differ in their phasic responses. Yet this, too, is unlikely. Leveraging a subset of the present

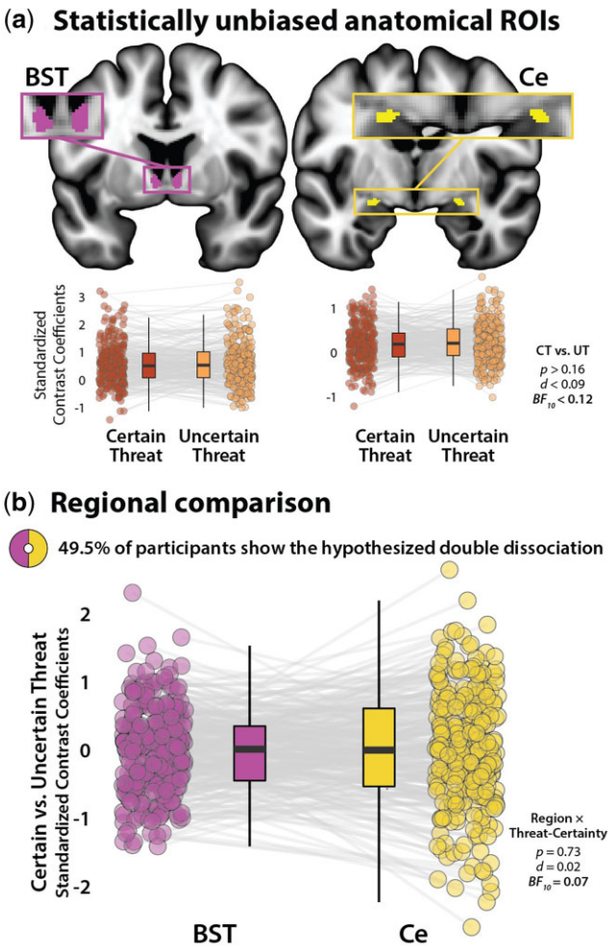

Figure 4 The human BST and Ce show statistically indistinguishable responses during certain- and uncertain-threat anticipation. (a) Anatomical ROIs. Probabilistic anatomical ROIs provided statistically unbiased estimates of BST and Ce activation during certain- and uncertain-threat anticipation. Leveraging spatially unsmoothed data, regression coefficients were extracted and averaged across voxels for each combination of ROI, task contrast, and participant. Box plots underscore negligible activation differences during the anticipation of certain-versus-uncertain threat in both the BST (left) and the Ce (right), contrary to double-dissociation models ($P>.16$, $d<0.09$, $BF_{10}<0.12$). Note: The y-axis scale differs across ROIs. (b) Regional comparison. A standard repeated-measures GLM was used to directly assess potential regional differences in reactivity to certain-versus-uncertain threat. Contrary to the double-dissociation model, the Region × Threat-Certainty interaction was not significant. Boxplot depicts the interaction as a 1-*df* contrast, that is, the "difference of differences." Participants were just as likely as not (49.5% vs. 50.5%) to show the hypothesized double dissociation, Z_{Sign} = 0.12, P = .91. Boxplots depict the median (*horizontal lines*), interquartile range (*boxes*), and individual participants (*dots*) for each contrast. Whiskers indicate 1.5× the interquartile range. Gray lines depict the sign and magnitude of intra-individual mean differences. Inset ring plot depicts the percentage of participants showing the hypothesized dissociation of regional reactivity to threat (BST: Certain < Uncertain Threat; Ce: Certain > Uncertain Threat). Abbreviations: BF, Bayes Factor; BST, bed nucleus of the stria terminalis; Ce, central nucleus of the amygdala; CT, certain-threat anticipation; *d*, Cohen's *d*. fMRI, functional magnetic resonance imaging; FWE, family-wise error; GLM, general linear model; ROI, region-of-interest; UT, uncertain-threat anticipation. AQ19 AQ20

sample ($n = 220$) and more sophisticated hemodynamic models, Cornwell and colleagues found statistically indistinguishable responses to anticipated threat, manifesting as sustained levels of heightened Ce/BST activation to temporally uncertain-and-distal encounters and phasic surges of Ce/BST activation to certain-and-imminent encounters (Cornwell *et al.* 2025). Taken together, this pattern of results reinforces the conclusion that the Ce and BST respond similarly to temporally certain and uncertain threat.

The similarities in Ce and BST function identified here are consistent with other evidence. Both regions are characterized by similar anatomical connectivity, cellular composition, neurochemistry, and gene expression (Fox *et al.* 2015b). Both are poised to trigger behavioral, psychophysiological, and neuroendocrine responses to threat via dense projections to downstream effector regions (Fox *et al.* 2015b). Activity in both regions has been shown to co-vary with individual differences in trait anxiety in large-scale studies of nonhuman primates ($n = 592$) (Fox *et al.* 2015a). Among humans, the Ce and BST are recruited by a broad spectrum of threatening and aversive stimuli (Fox and Shackman 2019, Hur *et al.* 2020, Shackman and Fox 2021) and both regions show hyper-reactivity to emotional tasks in individuals with anxiety disorders (Chavanne and Robinson 2021, Shackman and Fox 2021). Mechanistic work in rodents demonstrates that microcircuits within and between the Ce and BST are critical governors of defensive responses to both certain and uncertain threats (Lange *et al.* 2017, Fox and Shackman 2019, Pomrenze *et al.* 2019a, 2019b, Ressler *et al.* 2020, Chen *et al.* 2022, Holley and Fox 2022, Moscarello and Penzo 2022, Ren *et al.* 2022, Zhu *et al.* 2024). In fact, work in mice using a variant of the MTC shows that projections from the Ce to the BST are necessary for mounting defensive responses to temporally uncertain threat (Lange *et al.* 2017), dovetailing with the present results. Although our understanding remains far from complete, this body of work underscores the need to reformulate conceptual models that posit a strict functional segregation of certain and uncertain threat processing in the EA.

These observations do not mean that the Ce and BST are functionally identical or interchangeable. Indeed, our results indicate that the BST is more strongly recruited by both kinds of anticipated threat. Work in monkeys demonstrates that BST activity is more closely related to heritable variation ("nature") in trait anxiety, whereas Ce activity is more closely related to the variation in trait anxiety that is explained by differences in early-life experience ("nurture") (Fox *et al.* 2015a). The BST also appears to be more closely involved in organizing persistent signs of fear and anxiety following threat encounters (Duvarci *et al.* 2009, Shackman *et al.* 2017). Among humans, individual differences in neuroticism/negative emotionality, a prominent risk factor for anxiety disorders and depression, is selectively associated with heightened BST reactivity to uncertain-threat anticipation, an association that remains evident when controlling for Ce reactivity (Grogans *et al.* 2024). Clarifying the nature of these regional differences is an important avenue for future research. This endeavor is likely to benefit from the use of pharmacological challenges (e.g. acute benzodiazepine; Miles *et al.* 2011, Ressler *et al.* 2020) and theory-driven computational modeling (Holley and Fox 2022), approaches that would facilitate the development of coordinated cross-species models of fear and anxiety. When combined with parametric manipulations of specific facets of threat (e.g. duration, probability), computational modeling has the potential to address fundamental questions about the function of threat-sensitive brain regions, clarify inconsistencies across paradigms, and foster a common mathematical framework ("*lingua franca*") for integrating research across investigators, readouts, and species (Drzewiecki and Fox 2024).

The processing of uncertain and certain anticipated threats is not confined to the EA. Whole-brain voxelwise analyses revealed a distributed network that encompasses both frontocortical (MCC, AI/FrO, and dlPFC/FP) and other subcortical regions (PAG) regions (Fig. 3). And while this network is sensitive to both kinds of threat, with co-localization evident in every key region, direct comparison of the two threat conditions revealed greater frontocortical activation during uncertain-threat anticipation. We previously hypothesized that this could reflect differences in either cognitive load or the intensity of distress and arousal across conditions (Hur *et al.* 2020). On certain-threat trials, the descending integer stream ("countdown") provides an overt index of momentary changes in threat imminence. On uncertain-threat trials, this cognitive scaffolding is absent, encouraging reliance on the kinds of sustained, endogenous representations that are the hallmark of frontocortical regions (Tardiff and Curtis 2025). A second notable difference between the two threat conditions is the greater intensity of distress and arousal elicited by uncertain threat (Fig. 2), potentially reflecting differences in the cumulative hazard rate (i.e. the mathematical probability of encountering threat, given that it has not yet occurred) across the two threat conditions (Holley *et al.* 2024). From this perspective, increased frontocortical activation could reflect either heightened fear/anxiety or stronger recruitment of compensatory processes aimed at downregulating negative affect. On the one hand, there is ample evidence that frontocortical regions, including the MCC and AI/FrO, are recruited by a wide variety of aversive challenges, consistent with a role in *generating* negative affect (Xu *et al.* 2020, Chavanne and Robinson 2021, Bo *et al.* 2024, Radua *et al.* 2025). Of course, they also play a role in *regulating* distress (Bo *et al.* 2024). In laboratory studies of prompted cognitive reappraisal, MCC and dlPFC/FP activation scales with the degree of regulatory success (Urry *et al.* 2009, Bo *et al.* 2024), raising the possibility that frontocortical activation during aversive laboratory challenges partially reflects spontaneous efforts to downregulate or inhibit distress ("implicit" regulation; Shackman and Lapate 2018). Consistent with this hypothesis, we recently showed that heightened MCC and FrO reactivity to the MTC paradigm is associated with dampened emotional reactivity to real-world stressors, indexed using ecological momentary assessment (Hur *et al.* 2022), an observation that is consistent with evidence that loss of MCC function is associated with increased ("dysregulated") emotional reactivity to painful stimuli in humans and amplified defensive responses to threat in monkeys (Davis *et al.* 1994, Greenspan *et al.* 2008, Rahman *et al.* 2021).

Clearly, several challenges remain for the future. First, it will be important to determine whether our conclusions generalize to more demographically representative samples, other types of experimental threat (e.g. social), other kinds of uncertainty (e.g. probability, risk, ambiguity), and more naturalistic paradigms that span longer and more ecologically valid periods of threat anticipation (Wang *et al.* 2005, Mobbs *et al.* 2021). It merits comment that the absence of reward trials precludes strong inferences about valence. Second, the Ce and BST are complex and can be subdivided into multiple subdivisions, each containing intermingled cell types with distinct, even opposing functional roles (e.g. anxiogenic vs. anxiolytic) (Fox and Shackman 2019, 2024, Holley and Fox 2022, Moscarello and Penzo 2022). Animal models will be critical for generating testable hypotheses about the most relevant molecules, cell types, and microcircuits

(Fox and Shackman 2019, 2024, Kamboj *et al.* 2024). Third, fear and anxiety reflect the coordinated interactions of widely distributed neural networks (Tovote *et al.* 2015, Liu *et al.* 2024). Moving forward, it will be important to clarify the relevance of functional connectivity within and beyond the EA.

Anxiety disorders impose a staggering burden on global health, afflicting ∼360 million individuals annually (GBD2021 2024). Existing treatments were developed decades ago and have limited efficacy, acceptability, durability, and tolerability (Singewald *et al.* 2023, Cuijpers *et al.* 2024, De Crescenzo *et al.* 2024). Rising to this challenge requires the development of more accurate models of the neural systems governing fear and anxiety in health and disease. Leveraging a well-powered mega-analytic sample, translationally relevant fMRI paradigm, and best-practices analytic approach, the present results demonstrate that the EA systems recruited by certain and uncertain threat are not categorically different, with clear evidence of functional colocalization—*not* segregation—in the Ce and BST. These observations provide an empirically grounded framework for conceptualizing fear and anxiety, for understanding the functional neuroanatomy of threat processing in humans, and for accelerating the development of improved biological interventions for the suffering caused by extreme fear and anxiety.

Acknowledgements

The authors acknowledge the assistance and critical feedback from D. Bradford, J. Curtin, L. Friedman, C. Lejuez, B. Nacewicz, L. Pessoa, S. Rose, members of the Affective and Translational Neuroscience laboratory, the staff of the Maryland Neuroimaging Center, and the Office of the Registrar at the University of Maryland.

Author contributions

Paige Didier (Conceptualization [equal], Formal analysis [equal], Writing—original draft [equal], Writing—review & editing [equal]), Shannon E. Grogans (Writing—original draft [equal], Writing—review & editing [equal]), Claire M. Kaplan (Data curation [equal], Investigation [equal], Project administration [equal], Writing—review & editing [equal]), Hyung Cho Kim (Data curation [equal], Investigation [equal], Visualization [equal], Writing—review & editing [equal]), Samiha Islam (Data curation [equal], Investigation [equal], Project administration [equal], Writing—review & editing [equal]), Allegra S. Anderson (Formal analysis [equal], Investigation [equal], Writing—review & editing [equal]), Rachael M. Tillman (Investigation [equal], Writing—review & editing [equal]), Manuel Kuhn (Formal analysis [equal], Software [equal], Writing—review & editing [equal]), Juyoen Hur (Formal analysis [equal], Writing—review & editing [equal]), Andrew Fox (Investigation [equal], Writing—original draft [equal], Writing—review & editing [equal]), Kathryn A. DeYoung (Conceptualization [equal], Data curation [equal], Project administration [equal], Writing—review & editing [equal]), Jason F. Smith (Conceptualization [equal], Data curation [equal], Formal analysis [equal], Methodology [equal], Software [equal], Writing—original draft [equal], Writing—review & editing [equal]), Alexander J. Shackman (Conceptualization [equal], Formal analysis [equal], Funding acquisition [equal], Methodology [equal], Supervision [equal], Writing—original draft [equal], Writing—review & editing [equal])

Supplementary material

Supplementary material is available at *SCAN* online. AQ10

Conflicts of interest

None declared.

Funding

This work was partially supported by the California National Primate Center; National Institutes of Health (AA030042, AA031261, DA040717, MH018921, MH107444, MH121409, MH121735, MH128336, MH129851, OD011107, MH131264, MH132280, MH126426), University of California, Davis; and University of Maryland. AQ11

Data availability

Processed data, anatomical regions-of-interest, statistical code, and detailed results are available (https://osf.io/fcvdj). Task materials (https://osf.io/e2ngf) and key neuroimaging maps are also available (https://neurovault.org/collections/16083).

References

Ahrens S, Wu MV, Furlan A *et al.* A central extended amygdala circuit that modulates anxiety. *J Neurosci* 2018;**38**:5567–83. https://doi.org/10.1523/JNEUROSCI.0705-18.2018 AQ12

APA. *Diagnostic and Statistical Manual of Mental Disorders, Text Revision (DSM-5-TR)* (5 ed.). American Psychiatric Publishing, 2022. AQ13

Avery SN, Clauss JA, Blackford JU. The human BNST: functional role in anxiety and addiction. *Neuropsychopharmacology* 2016;**41**:126–41. https://doi.org/10.1038/npp.2015.185

Blanchard DC, Canteras NS. In search of the behavioral and neural basis for differentiating fear and anxiety. *Biol Psychiatry Glob Open Sci* 2024;**4**:394–5. https://doi.org/10.1016/j.bpsgos.2023.05.008

Bo K, Kraynak TE, Kwon M *et al.* A systems identification approach using Bayes factors to deconstruct the brain bases of emotion regulation. *Nat Neurosci* 2024;**27**:975–87. https://doi.org/10.1038/s41593-024-01605-7

Bruzsik B, Biro L, Zelena D *et al.* Somatostatin neurons of the bed nucleus of stria terminalis enhance associative fear memory consolidation in mice. *J Neurosci* 2021;**41**:1982–95. https://doi.org/10.1523/jneurosci.1944-20.2020

Chavanne AV, Robinson OJ. The overlapping neurobiology of adaptive and pathological anxiety: a meta-analysis of functional neural activation. *Am J Psychiatry* 2021;**178**:156–64. https://doi.org/10.1176/appi.ajp.2020.19111153

Chen WH, Lien CC, Chen CC. Neuronal basis for pain-like and anxiety-like behaviors in the central nucleus of the amygdala. *Pain* 2022;**163**:e463–75. https://doi.org/10.1097/j.pain.0000000000002389

Choi JM, Padmala S, Pessoa L. Impact of state anxiety on the interaction between threat monitoring and cognition. *Neuroimage* 2012;**59**:1912–23.

Cohen J. *Statistical Power Analysis for the Behavioral Sciences* (2nd ed.). Lawrence Erlbaum Associates, 1988. AQ14

Cohen JR. The earth is round ($p < .05$). *Am Psychol* 1994;**49**:997–1003. https://doi.org/10.1037/0003-066X.49.12.997

Cornwell BR, Didier PR, Grogans SE *et al.* A shared threat-anticipation circuit is dynamically engaged at different moments by certain and

uncertain threat. *J Neurosci* 2025;**45**:e2113242025. https://doi.org/10.1523/JNEUROSCI.2113-24.2025

Costafreda SG. Pooling FMRI data: meta-analysis, mega-analysis and multi-center studies. *Front Neuroinform*, 2009;**3**:33. https://doi.org/10.3389/neuro.11.033.2009

Cuijpers P, Miguel C, Ciharova M *et al.* Absolute and relative outcomes of psychotherapies for eight mental disorders: a systematic review and meta-analysis. *World Psychiatry* 2024;**23**:267–75. https://doi.org/10.1002/wps.21203

Daniel-Watanabe L, Fletcher PC. Are fear and anxiety truly distinct? *Biol Psychiatry Glob Open Sci* 2022;**2**:341–9. https://doi.org/10.1016/j.bpsgos.2021.09.006

Davis KD, Hutchison WD, Lozano AM *et al.* Altered pain and temperature perception following cingulotomy and capsulotomy in a patient with schizoaffective disorder. *Pain* 1994;**59**:189–99. https://doi.org/0304-3959(94)90071-X [pii]

De Crescenzo F, De Giorgi R, Garriga C *et al.* Real-world effects of antidepressants for depressive disorder in primary care: population-based cohort study. *Br J Psychiatry* 2024;**226**:1–10. https://doi.org/10.1192/bjp.2024.194

Drzewiecki CM, Fox AS. Understanding the heterogeneity of anxiety using a translational neuroscience approach. *Cogn Affect Behav Neurosci*, 2024;**24**:228–45. https://doi.org/10.3758/s13415-024-01162-3

Duvarci S, Bauer EP, Paré D. The bed nucleus of the stria terminalis mediates inter-individual variations in anxiety and fear. *J Neurosci* 2009;**29**:10357–61. https://doi.org/29/33/10357 [pii] https://doi.org/10.1523/JNEUROSCI.2119-09.2009

*Faul F, Erdfelder E, Lang A-G *et al.* GPower 3: a flexible statistical power analysis program for the social, behavioral, and biomedical sciences. *Behav Res Methods* 2007;**39**:175–91.

Fox AS, Lapate RC, Davidson RJ, Shackman AJ. The nature of emotion: a research agenda for the 21st century. In AS Fox, RC Lapate, AJ Shackman, RJ Davidson (eds.), *The Nature of Emotion. Fundamental Questions* (2nd ed.). Oxford University Press, 2018, 403–417.

Fox AS, Oler JA, Shackman AJ *et al.* Intergenerational neural mediators of early-life anxious temperament. *Proc Natl Acad Sci U S A* 2015a; **112**:9118–22.

Fox AS, Oler JA, Tromp DP *et al.* Extending the amygdala in theories of threat processing. *Trends Neurosci* 2015b;**38**:319–29. https://doi.org/10.1016/j.tins.2015.03.002

Fox AS, Shackman AJ. The central extended amygdala in fear and anxiety: closing the gap between mechanistic and neuroimaging research. *Neurosci Lett* 2019;**693**:58–67. https://doi.org/10.1016/j.neulet.2017.11.056

Fox AS, Shackman AJ. An honest reckoning with the amygdala and mental illness. *Am J Psychiatry* 2024;**181**:1059–75. https://doi.org/10.1176/appi.ajp.20240941

Freud S, Strachey J, Freud A *et al. The* Standard Edition of the Complete Psychological Works of Sigmund Freud, Volume 20 (1925-1926): An Autobiographical Study, Inhibitions, Symptoms and Anxiety, the Question of Lay Analysis and Other Works. Hogarth Press, 1959.

GBD2021 Global incidence, prevalence, years lived with disability (YLDs), disability-adjusted life-years (DALYs), and healthy life expectancy (HALE) for 371 diseases and injuries in 204 countries and territories and 811 subnational locations, 1990-2021: a systematic analysis for the Global Burden of Disease Study 2021. *Lancet* 2024; **403**:2133–61. https://doi.org/10.1016/S0140-6736(24)00757-8

Greenspan JD, Coghill RC, Gilron I *et al.* Quantitative somatic sensory testing and functional imaging of the response to painful stimuli before and after cingulotomy for obsessive-compulsive disorder (OCD). *Eur J Pain* 2008;**12**:990–9. https://doi.org/10.1016/j.ejpain.2008.01.007

Griessner J, Pasieka M, Bohm V *et al.* Central amygdala circuit dynamics underlying the benzodiazepine anxiolytic effect. *Mol Psychiatry* 2021;**26**:534–44. https://doi.org/10.1038/s41380-018-0310-3

Grillon C, Ernst M. A way forward for anxiolytic drug development: Testing candidate anxiolytics with anxiety-potentiated startle in healthy humans. *Neurosci Biobehav Rev* 2020;**119**:348–54. https://doi.org/10.1016/j.neubiorev.2020.09.024

Grogans SE, Bliss-Moreau E, Buss KA *et al.* The nature and neurobiology of fear and anxiety: State of the science and opportunities for accelerating discovery. *Neurosci Biobehav Rev* 2023;**151**:105237. https://doi.org/10.1016/j.neubiorev.2023.105237

Grogans SE, Hur J, Barstead MG *et al.* Neuroticism/negative emotionality is associated with increased reactivity to uncertain threat in the bed nucleus of the stria terminalis, not the amygdala. *J Neurosci* 2024;**44**: e1868232024.

Gronau QF, Ly A, Wagenmakers E-J. Informed Bayesian t-tests. *Am Stat* 2020;**74**:137–43. https://doi.org/10.1080/00031305.2018.1562983

Grupe DW, Nitschke JB. Uncertainty and anticipation in anxiety: an integrated neurobiological and psychological perspective. *Nat Rev Neurosci* 2013;**14**:488–501. https://doi.org/nrn3524 [pii] https://doi.org/10.1038/nrn3524

Grupe DW, Wielgosz J, Davidson RJ *et al.* Neurobiological correlates of distinct post-traumatic stress disorder symptom profiles during threat anticipation in combat veterans. *Psychol Med* 2016;**46**: 1885–95. https://doi.org/10.1017/S0033291716000374

Gungor NZ, Paré D. Functional heterogeneity in the bed nucleus of the stria terminalis. *J Neurosci* 2016;**36**:8038–49.

Holley D, Fox AS. The central extended amygdala guides survival-relevant tradeoffs: Implications for understanding common psychiatric disorders. *Neurosci Biobehav Rev* 2022;**142**:104879. https://doi.org/10.1016/j.neubiorev.2022.104879

Holley D, Varga EA, Boorman ED *et al.* Temporal dynamics of uncertainty cause anxiety and avoidance. *Computational Psychiatry*, 2024; **8**:85–91. https://doi.org/10.5334/cpsy.105

Hur J, Kuhn M, Grogans SE *et al.* Anxiety-related frontocortical activity is associated with dampened stressor reactivity in the real world. *Psychol Sci* 2022;**33**:906–24. https://doi.org/10.1101/2021.03.17.435791

Hur J, Smith JF, DeYoung KA *et al.* Anxiety and the neurobiology of temporally uncertain threat anticipation. *J Neurosci* 2020;**40**:7949–64. https://doi.org/10.1101/2020.02.25.964734

Kamboj S, Carlson EL, Ander BP *et al.* Translational insights from cell-type variation across amygdala subnuclei in rhesus monkeys and humans. *Am J Psychiatry* 2024;**181**:1086–102.

Kim HC, Kaplan CM, Islam S *et al.* Acute nicotine abstinence amplifies subjective withdrawal symptoms and threat-evoked fear and anxiety, but not extended amygdala reactivity. *PLoS One* 2023;**18**: e0288544. https://doi.org/10.1371/journal.pone.0288544

Klumpers F, Kroes MCW, Baas J *et al.* How human amygdala and bed nucleus of the stria terminalis may drive distinct defensive responses. *J Neurosci* 2017;**37**:9645–56. https://doi.org/10.1523/JNEUROSCI.3830-16.2017

Lange MD, Daldrup T, Remmers F *et al.* Cannabinoid CB1 receptors in distinct circuits of the extended amygdala determine fear responsiveness to unpredictable threat. *Mol Psychiatry* 2017;**22**:1422–30. https://doi.org/10.1038/mp.2016.156

LeDoux JE, Pine DS. Using neuroscience to help understand fear and anxiety: a two-system framework. *Am J Psychiatry* 2016;**173**: 1083–93. https://doi.org/10.1176/appi.ajp.2016.16030353

Lee SC, Amir A, Haufler D *et al.* Differential recruitment of competing valence-related amygdala networks during anxiety. *Neuron* 2017;**96**:81–8.e85. https://doi.org/10.1016/j.neuron.2017.09.002

Liu X, Jiao G, Zhou F *et al.* A neural signature for the subjective experience of threat anticipation under uncertainty. *Nat Commun* 2024;**15**:1544. https://doi.org/10.1038/s41467-024-45433-6

Marcinkiewcz CA, Mazzone CM, D'Agostino G *et al.* Serotonin engages an anxiety and fear-promoting circuit in the extended amygdala. *Nature* 2016;**537**:97–101. https://doi.org/10.1038/nature19318

Marvar PJ, Andero R, Hurlemann R *et al.* Limbic neuropeptidergic modulators of emotion and their therapeutic potential for anxiety and post-traumatic stress disorder. *J Neurosci* 2021;**41**:901–10. https://doi.org/10.1523/jneurosci.1647-20.2020

Miles L, Davis M, Walker D. Phasic and sustained fear are pharmacologically dissociable in rats. *Neuropsychopharmacology* 2011;**36**:1563–74. https://doi.org/10.1038/npp.2011.29

Mobbs D, Wise T, Suthana N *et al.* Promises and challenges of human computational ethology. *Neuron* 2021;**109**:2224–38. https://doi.org/10.1016/j.neuron.2021.05.021

Moscarello JM, Penzo MA. The central nucleus of the amygdala and the construction of defensive modes across the threat-imminence continuum. *Nat Neurosci* 2022;**25**:999–1008. https://doi.org/10.1038/s41593-022-01130-5

Murty D, Song S, Morrow K *et al.* Distributed and multifaceted effects of threat and safety. *J Cogn Neurosci* 2022;**34**:495–516. https://doi.org/10.1162/jocn_a_01807

Murty DVPS, Song S, Surampudi SG *et al.* Threat and reward imminence processing in the human brain. *J Neurosci* 2023;**43**:2973–87. https://doi.org/10.1523/jneurosci.1778-22.2023

Nichols T, Brett M, Andersson J *et al.* Valid conjunction inference with the minimum statistic. *Neuroimage* 2005;**25**:653–60. https://doi.org/S1053-8119(04)00750-5 [pii] https://doi.org/10.1016/j.neuroimage.2004.12.005

NIMH. (2011). *Negative valence systems: Workshop proceedings (March 13, 2011 – March 15, 2011; Rockville, Maryland).* Retrieved July 1 from https://www.nimh.nih.gov/research/research-funded-by-nimh/rdoc/negative-valence-systems-workshop-proceedings.shtml

Petre B, Kragel P, Atlas LY *et al.* A multistudy analysis reveals that evoked pain intensity representation is distributed across brain systems. *PLoS Biol* 2022;**20**:e3001620. https://doi.org/10.1371/journal.pbio.3001620

Poldrack RA, Baker CI, Durnez J *et al.* Scanning the horizon: towards transparent and reproducible neuroimaging research. *Nat Rev Neurosci* 2017;**18**:115–26.

Pomrenze MB, Giovanetti SM, Maiya R *et al.* Dissecting the roles of GABA and neuropeptides from rat central amygdala CRF neurons in anxiety and fear learning. *Cell Rep* 2019a;**29**:13–21 e14. https://doi.org/10.1016/j.celrep.2019.08.083

Pomrenze MB, Tovar-Diaz J, Blasio A *et al.* A corticotropin releasing factor network in the extended amygdala for anxiety. *J Neurosci* 2019b;**39**:1030–43. https://doi.org/10.1523/JNEUROSCI.2143-18.2018

Radua J, Savage HS, Vilajosana E *et al.* Neural correlates of human fear conditioning and sources of variability: an fMRI mega-analysis and normative modelling study of 2,199 individuals. *Nat Commun* 2025;**16**:7869.

Rahman SS, Mulvihill K, Wood CM *et al.* Differential contribution of anterior and posterior midcingulate subregions to distal and proximal threat reactivity in marmosets. *Cereb Cortex* 2021;**31**:4765–80. https://doi.org/10.1093/cercor/bhab121

Ren J, Lu CL, Huang J *et al.* A distinct metabolically defined central nucleus circuit bidirectionally controls anxiety-related behaviors. *J Neurosci* 2022;**42**:2356–70. https://doi.org/10.1523/jneurosci.1578-21.2022

Ressler RL, Goode TD, Evemy C *et al.* NMDA receptors in the CeA and BNST differentially regulate fear conditioning to predictable and unpredictable threats. *Neurobiol Learn Mem* 2020;**174**:107281. https://doi.org/10.1016/j.nlm.2020.107281

Salimi-Khorshidi G, Smith SM, Keltner JR *et al.* Meta-analysis of neuroimaging data: a comparison of image-based and coordinate-based pooling of studies. *Neuroimage* 2009;**45**:810–23. https://doi.org/S1053-8119(08)01290-1 [pii] https://doi.org/10.1016/j.neuroimage.2008.12.039

Salomon JA, Haagsma JA, Davis A *et al.* Disability weights for the Global Burden of Disease 2013 study. *Lancet Glob Health* 2015;**3**:e712-723–e723. https://doi.org/10.1016/S2214-109X(15)00069-8

Schimmack U. (2019). *Statistics wars: Don't change alpha. Change the null-hypothesis!* Retrieved December 15 from https://replicationindex.com/category/nil-hypothesis/

Schmalz X, Biurrun Manresa J, Zhang L. What is a Bayes factor? *Psychol Methods* 2023;**28**:705–18. https://doi.org/10.1037/met0000421

Schmitz A, Grillon C. Assessing fear and anxiety in humans using the threat of predictable and unpredictable aversive events (the NPU-threat test). *Nat Protoc* 2012;**7**:527–32. https://doi.org/nprot.2012.001 [pii] https://doi.org/10.1038/nprot.2012.001

Schönbrodt FD, Wagenmakers EJ, Zehetleitner M *et al.* Sequential hypothesis testing with bayes factors: Efficiently testing mean differences. *Psychol Methods* 2017;**22**:322–39. https://doi.org/10.1037/met0000061

Shackman AJ, Fox AS. Contributions of the central extended amygdala to fear and anxiety. *J Neurosci* 2016;**36**:8050–63. https://doi.org/10.1523/JNEUROSCI.0982-16.2016

Shackman AJ, Fox AS. Two decades of anxiety neuroimaging research: new insights and a look to the future. *Am J Psychiatry* 2021;**178**:106–9.

Shackman AJ, Fox AS, Oler JA *et al.* Heightened extended amygdala metabolism following threat characterizes the early phenotypic risk to develop anxiety-related psychopathology. *Mol Psychiatry* 2017;**22**:724–32.

Shackman AJ, Grogans SE, Fox AS. Fear, anxiety, and the functional architecture of the human central extended amygdala. *Nat Rev Neurosci* 2024;**25**:587–8. https://doi.org/10.1038/s41583-024-00832-y

Shackman AJ, Lapate RC. How are emotions regulated by context and cognition? In AS Fox, RC Lapate, AJ Shackman, RJ Davidson (eds.), *The Nature of Emotion. Fundamental Questions* (2nd ed.). Oxford University Press, 2018, 177–179.

Singewald N, Sartori SB, Reif A *et al.* Alleviating anxiety and taming trauma: novel pharmacotherapeutics for anxiety disorders and post-traumatic stress disorder. *Neuropharmacology* 2023;**226**:109418. https://doi.org/10.1016/j.neuropharm.2023.109418

Somerville LH, Wagner DD, Wig GS *et al.* Interactions between transient and sustained neural signals support the generation and regulation of anxious emotion. *Cereb Cortex* 2013;**23**:49–60. https://doi.org/10.1093/cercor/bhr373

Tardiff N, Curtis CE. Short-term and working memory. In J. Wixted (Ed.), *Learning and Memory: A Comprehensive Reference* (3rd ed.). Academic Press, 2025, 112–133. https://doi.org/10.1016/B978-0-443-15754-7.00025-0

Theiss JD, Ridgewell C, McHugo M *et al.* Manual segmentation of the human bed nucleus of the stria terminalis using 3T MRI. *Neuroimage* 2017;**146**:288–92. https://doi.org/10.1016/j.neuroimage.2016.11.047

Tillman RM, Stockbridge MD, Nacewicz BM *et al.* Intrinsic functional connectivity of the Central extended amygdala. *Hum Brain Mapp* 2018;**39**:1291–312.

Tovote P, Fadok JP, Lüthi A. Neuronal circuits for fear and anxiety. *Nat Rev Neurosci* 2015;**16**:317–31. https://doi.org/10.1038/nrn3945

Urry HL, van Reekum CM, Johnstone T *et al.* Individual differences in some (but not all) medial prefrontal regions reflect cognitive demand while regulating unpleasant emotion. *Neuroimage* 2009;**47**:852–63. https://doi.org/S1053-8119(09)00581-3 [pii] https://doi.org/10.1016/j.neuroimage.2009.05.069

van Doorn J, van den Bergh D, Böhm U *et al.* The JASP guidelines for conducting and reporting a Bayesian analysis. *Psychon Bull Rev* 2021;**28**:813–26. https://doi.org/10.3758/s13423-020-01798-5

Wagenmakers E-J, Love J, Marsman M *et al.* Bayesian inference for psychology. Part II: Example applications with JASP. *Psychon Bull Rev* 2018;**25**:58–76. https://doi.org/10.3758/s13423-017-1323-7

Wang J, Rao H, Wetmore GS *et al.* Perfusion functional MRI reveals cerebral blood flow pattern under psychological stress. *Proc Natl Acad Sci U S A* 2005;**102**:17804–9. https://doi.org/0503082102 [pii] https://doi.org/10.1073/pnas.0503082102

Xu A, Larsen B, Baller EB *et al.* Convergent neural representations of experimentally-induced acute pain in healthy volunteers: a large-scale fMRI meta-analysis. *Neurosci Biobehav Rev* 2020;**112**:300–23. https://doi.org/10.1016/j.neubiorev.2020.01.004

Zhu Y, Xie SZ, Peng AB *et al.* Distinct circuits from the central lateral amygdala to the ventral part of the bed nucleus of stria terminalis regulate different fear memory. *Biol Psychiatry* 2024;**95**:732–44. https://doi.org/10.1016/j.biopsych.2023.08.022

Supplementary Materials

Paige R. Didier[1]
Shannon E. Grogans[1]
Claire M. Kaplan[4]
Hyung Cho Kim[2,3]
Samiha Islam[5]
Allegra S. Anderson[6]
Rachael M. Tillman[7]
Manuel Kuhn[8]
Juyoen Hur[9]
Andrew S. Fox[10,11]
Kathryn A. DeYoung[1]
Jason F. Smith[1]
Alexander J. Shackman[1,2,3]

Department of [1]Psychology, [2]Neuroscience and Cognitive Science Program, and [3]Maryland Neuroimaging Center, University of Maryland, College Park, MD 20742 USA. [4]CommonSpirit Neuropsychology, Lakewood, CO 80228 USA. [5]Rees-Jones Center for Foster Care Excellence, Children's Heath, Dallas, TX 75207 USA. [6]Department of Psychiatry and Human Behavior, Brown University, Providence, RI 02912 USA. [7]McGill Neuropsychology, Bethesda, MD 20814 USA. [8]Institute of Medical Psychology, Charité Universitätsmedizin Berlin, 10117 Berlin, Germany. [9]Department of Psychology, Yonsei University, Seoul 03722, Republic of Korea. [10]Department of Psychology and [11]California National Primate Research Center, University of California, Davis, CA 95616 USA

Please address manuscript correspondence to

Alexander J. Shackman (shackman@umd.edu)

SUPPLEMENTARY NOTE 1. ***Fear, anxiety, and the extended amygdala.***

In this section, we briefly highlight some prominent neuroscientific definitions of fear and anxiety and recent theoretical claims about the functional organization of the two major subdivisions of the extended amygdala (EA), including the central nucleus of the amygdala (Ce/CeA) and the bed nucleus of the stria terminalis (BST/BNST).

By design, this brief survey is meant to be illustrative, *not* comprehensive. For a panel discussion of related conceptual issues, see Grogans and colleagues (Grogans et al., 2023). For an overview of popular assays for assessing fear and anxiety in different species, see Shackman and colleagues (Shackman et al., 2016). For an overview of concerns centered on the imprecision and inconsistency of fear-and-anxiety terminology see Perusini and Fanselow (Perusini & Fanselow, 2015) and Shackman and Fox (Shackman & Fox, 2016).

Avery et al. *Neuropsychopharmacology* 2016 (Avery et al., 2016)

- *"The amygdala mediates short-term, phasic responses to immediate threats, whereas the BNST mediates sustained responses to contextual, diffuse, and unpredictable threats."*

Daniel-Watanabe & Fletcher *Biological Psychiatry Global Open Science* 2022 (Daniel-Watanabe & Fletcher, 2022)

- *"Fear is related to the presence, or imminent presence, of the aversive stimulus, while anxiety is considered the more protracted state produced by a sustained expectation that the aversive event is likely to occur."*

- *"Evidence that both amygdala and BNST are responsive to both predictable and unpredictable threats… calls into question this overall claim for a neural distinction between fear and anxiety."*

- *"It is difficult to escape the conclusion that the current distinction between fear and anxiety is an unreliable one. While it has been useful in guiding research and clinical work, the inconsistencies suggest that there is a need to reexamine the distinction and consider the importance of other aspects of the experience of anxiety, such as uncertainty and avoidance."*

Davis et al. *Neuropsychopharmacology* 2010 (Davis et al., 2010)

- *"Although the symptoms of fear and anxiety are very similar, they differ in terms of certain key dimensions….Fear is prompted by imminent and real danger, and galvanizes active defensive responses. In contrast, anxiety is often elicited by less specific and less predictable threats, or by those that are physically or psychologically more distant."*

- *"The BLA [basolateral amygdala] sends heavy projections to both the CeA and the BNST… The heaviest projections…are to the* CeA_M *[medial division of the Ce/CeA], which in turn projects to the hypothalamus and brainstem to mediate phasic fear responses…A long duration fear stimulus*

activates the BLA, which then rapidly activates the CeA_M to produce phasic fear through the release of glutamate acting on AMPA/kainate receptors on CeA_M neurons. Shortly thereafter, inputs to the CeA_L [lateral division of the Ce/CeA] then release CRF into the BNST to cause a long-lasting sustained fear reaction. Inhibitory feedback to the CeA_M from either the CeA_L or the BNST shuts down the CeA_M, allowing a seamless transition from phasic to sustained fear.

Domschke *Biological Psychiatry Global Open Science* 2022 (Domschke, 2022)

- *"Fear and anxiety seem to represent closely interrelated diagnostic constructs remaining to be further interrogated for their shared and unique molecular, neuronal, physiological, and behavioral substrates—quite in accordance with Martin Heidegger's reconciling notion:* "Of course it still remains obscure how [anxiety] is connected ontologically with fear. Obviously these are kindred phenomena."

Fox & Shackman *Neuroscience Letters* 2019 (Fox & Shackman, 2019)

- *"On balance, the brain imaging literature suggests that the Ce and BST, while certainly not interchangeable, are more alike than different."*

- *"The central extended amygdala plays a crucial role in evaluating and responding to a broad spectrum of threat-related cues and contexts. While they are certainly not interchangeable, the Ce and the BST show similar patterns of connectivity, cellular composition, neurochemistry, and gene expression. Both are sensitive to uncertain or temporally remote threat; both co-vary with threat-elicited changes in behavior, physiology, and experience; both show phasic responses to acute threat; and both show heightened activity during sustained exposure to diffusely threatening contexts. Work in rodents indicates that both regions play a critical role in organizing sustained defensive responses to a range of potentially threatening cues and contexts."*

Grupe & Nitschke *Nature Reviews Neuroscience* 2013 (Grupe & Nitschke, 2013)

- *"Fear and anxiety can be distinguished according to how much certainty one has regarding the likelihood, timing or nature of a future threat…Environmental cues indicating the unambiguous presence of an immediate threat give rise to intense 'fearful' defensive behaviours (that is, 'fight or flight'), whereas more diffuse, distal or unpredictable threat cues produce 'anxious' risk assessment behaviour…that is likely to persist until such uncertainty is resolved."*

- *"We define anxiety…as anticipatory affective, cognitive and behavioural changes in response to uncertainty about a potential future threat."*

Gungor & Paré *Journal of Neuroscience* 2016 (Gungor & Paré, 2016)

- *Early work stressed the differing involvement of the central amygdala (CeA) and bed nucleus of the stria terminalis (BNST) in the genesis of fear versus anxiety, respectively…This model became extremely influential and now guides a new wave of studies on the role of BNST in humans. Here, we consider evidence for and against this model…This analysis leads us to conclude that BNST's influence is not limited to the generation of anxiety-like responses to diffuse threats, but that it also shapes the impact of discrete threatening stimuli."*

LeBow & Chen *Molecular Psychiatry* 2016 (Lebow & Chen, 2016)

- *"The amygdala is responsible for mediating specific cue-based fear responses, and thus controls the assessment of immediate or phasic fear."*

- *"Fear and anxiety can be divided into an immediate threat, for example, the presence of a predator, and pre- or post-encounter threats, for example, the apprehension of encountering a predator again. The BNST is hypothesized to mediate these longer-term responses to anxiety, where a challenge or recovery from a challenge to homeostasis occurs. In contrast, the CeA is thought to mediate shorter duration phasic fear responses, which occur in response to a current challenge to homeostasis."*

LeDoux & Pine *American Journal of Psychiatry* 2016 (LeDoux & Pine, 2016)

- *"We propose…that the mental state term* fear *be used to describe feelings that occur when the source of harm, the threat, is either immediate or imminent, and* anxiety *be used to describe feelings that occur when the source of harm is uncertain or is distal in space or time."*

- *"Just as findings demonstrating that the amygdala detects and controls behavioral and physiological responses to immediate threats have supported views of the amygdala as fear-circuit hub, other findings, about responses to uncertain threats, have led to a view of the circuitry of anxiety. Thus, in recent years, animal research has suggested the bed nucleus of the stria terminalis (BNST) is engaged when threats are uncertain…resulting in behavioral inhibition and risk assessment …The BNST has thus come to be for anxiety what the amygdala is for fear—a circuit hub out of which anxious feelings emerge."*

Mobbs et al. *Trends in Cognitive Sciences* 2020 (Mobbs et al., 2020)

- *"Anxiety: a future-oriented emotional state associated with potential and uncertain threats."*

- *"Fear: an emotion that is associated with a present and identifiable threat."*

Moscarello & Penzo *Nature Neuroscience* 2022 (Moscarello & Penzo, 2022)

- *In nature, animals display defensive behaviors that reflect the spatiotemporal distance of threats. Laboratory-based paradigms that elicit specific defensive responses in rodents have provided valuable insight into the brain mechanisms that mediate the construction of defensive modes with varying degrees of threat imminence….High- and low-imminence defensive modes…are mediated at the neural-circuit level within the CeA and its downstream targets.*

NIMH *Negative Valence Systems: Workshop Proceedings* 2011 (NIMH, 2011)

- *"Responses to acute threat (Fear): Activation of the brain's defensive motivational system to promote behaviors that protect the organism from perceived danger. Normal fear involves a pattern of adaptive responses to conditioned or unconditioned threat stimuli (exteroceptive or interoceptive). Fear can involve internal representations and cognitive processing, and can be modulated by a variety of factors."*

- *"Responses to potential harm (Anxiety): Activation of a brain system in which harm may potentially occur but is distant, ambiguous, or low/uncertain in probability, characterized by a pattern of responses such as enhanced risk assessment (vigilance). These responses to low imminence threats are qualitatively different than the high imminence threat behaviors that characterize fear."*

- *"While there is considerable overlap in the efferent activity generated, the distinction between these two constructs has found support in both animal and human literatures. In animal models, acute threat is associated with efferent activity from the amygdala, whereas potential harm has been shown to be related to activation of the bed nucleus of the stria terminalis (BNST)."*

——— Units of Analysis ———			
Genes	**Molecules**	**Cells**	**Circuits**
Construct: Acute Threat ("Fear")			
BDNF, 5HT/5HTRs, CRF, FKB5, GABAARs, Glutamate system, NMDARs, Opioid system, COMT, Cannabinoid system, Dopamine, DAT, Cam kinase, MAP kinase, PI-3 kinase, PKA, PKC, Acetylcholine, Norepinephrine, Strathmin, Pkap, TRBC5	NMDAR, Glutamate, Dopamine, Serotonin, BDNF, GABA, Cortisol/ Corticosterone, Endogenous cannabinoids, orexin, NPY, CRF family, FGF2, Oxytocin, Vasopressin, CCK, Neuropeptide S, Neurosteroids	Neurons, Glia, Pyramidal cells, GABAergic cells	Central Nucleus, BasAmyg, LatAmyg, vPAG, dPAG, v-hippocampus (post), d-hippocampus (ant), latPFC/insula, vmPFC (il), dmPFC (pl), OFC, Hypothalamus, dorsal ACC, rostral/vent ACC, ICMs, Medial Amyg, PAG, RPVM, Pons, autonomic nervous system, insular cortex, LC
Construct: Potential Harm ("Anxiety")			
CRF	CRF family, cortisol	Pituitary cells	Bed nucleus of stria terminalis

Oredu, Lennon, Vervliet & Schiller (Orederu et al., 2024)

- *"Ethological, clinical, and neurobiological evidence strongly suggests that what we colloquially call "fear" is best understood as referring to two different scientific constructs, namely fear and anxiety…Fear is a transient reaction to an identifiable and often proximal threat…and serves to motivate defensive behaviors aimed at coping with the upcoming threat (e.g., fight, flight, freeze). Anxiety, on the other hand, refers to more general, chronic apprehension and worry that is free-floating and not bound to a specific object…Essentially, fear constitutes a state in which a person is actively responding to present danger, while anxiety refers to a person's response to an uncertain threat that may occur in the future."*

- *"Inactivation of…BNST selectively impairs innate, but not conditioned, fear responses…These roles are reversed when it comes to conditioned fear, with central nucleus inactivation leading to selective reduction in conditioned fear, and BNST…inactivation sparing conditioned fear…Such divergent findings point to a specific role for the central nucleus in conditioned fear."*

Tovote et al. *Nature Reviews Neuroscience* 2015 (Tovote et al., 2015)

- *"Whereas fear is evoked by discrete and acutely threatening stimuli, anxiety can be operationalized as an emotional response to vague, potential threats."*

SUPPLEMENTARY FIGURES AND CAPTIONS

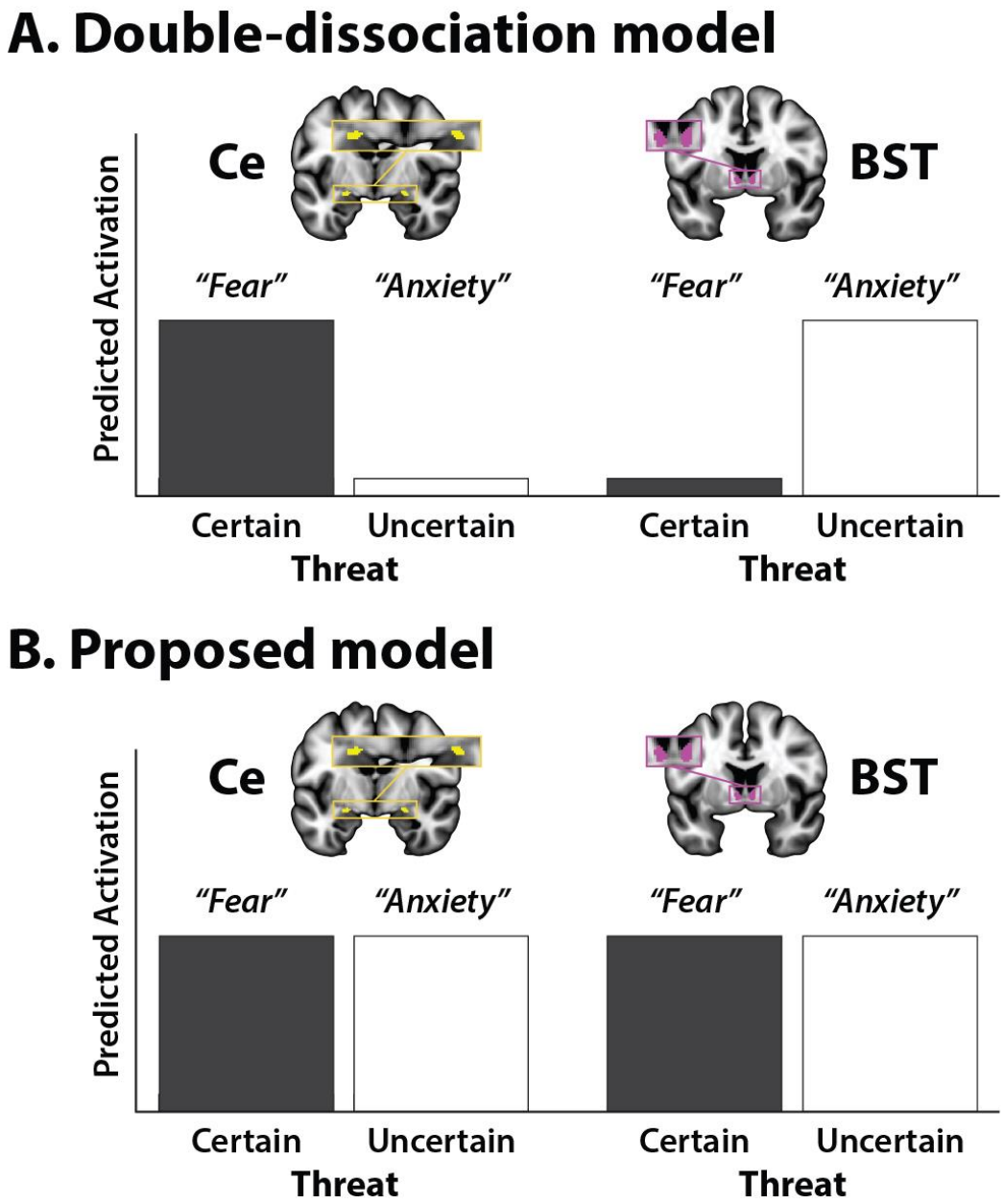

Supplementary Figure S1. Conceptual overview of competing hypotheses about the functional architecture of the extended amygdala (EA). **(A)** ***Double-dissociation model.*** Several influential models suggest that fear and anxiety arise from two strictly segregated, doubly dissociable neural systems, positing that the Ce is sensitive to certain (but not uncertain) threat and promotes signs and symptoms of fear; whereas the BST is sensitive to uncertain (but not certain) threat and promotes anxiety (see **Supplementary Note 1**, above). **(B)** ***Proposed model.*** We propose a competing hypothesis, positing that that the Ce and BST play a role in governing responses to both kinds of threat (Fox & Shackman, 2019; Shackman & Fox, 2016). Note: This figure is purely for heuristic purposes and does not depict actual data. Abbreviations—BST, bed nucleus of the stria terminalis; Ce, central nucleus of the amygdala.

SUPPLEMENTARY METHOD

Threat-Anticipation Paradigm

Paradigm Structure and Design Considerations. The Maryland Threat Countdown paradigm is a well-established, fMRI-optimized variant of temporally uncertain-threat assays that have been validated in rodents and humans (Daldrup et al., 2015; Hefner et al., 2013; Lange et al., 2017; Miles et al., 2011; Moberg et al., 2017).

As shown schematically in **Figure 1**, the paradigm takes the form of a 2 (*Valence:* Threat/Safety) × 2 (*Temporal Certainty:* Uncertain/Certain) randomized, event-related, repeated-measures design (3 scans; 6 trials/condition/scan). Participants were completely informed about the task design and contingencies prior to scanning. Simulations were used to optimize the detection and deconvolution of task-related hemodynamic signals. Stimulus presentation was controlled using Presentation software (version 19.0, Neurobehavioral Systems, Berkeley, CA).

On Certain-Threat trials, participants saw a descending stream of integers ('count-down;' e.g., 30, 29, 28...3, 2, 1) for 18.75 s. To ensure robust distress and arousal, the anticipation epoch culminated with the presentation of a noxious electric shock, unpleasant photograph (e.g., mutilated body), and thematically related audio clip (e.g., gunshot). Uncertain-Threat trials were similar, but the integer stream was randomized and presented for an uncertain and variable duration (8.75-30.00 s; *M*=18.75 s). Here, participants knew that something aversive was going to occur but had no way of knowing precisely when. Consistent with methodological recommendations (Shackman & Fox, 2016), the mean duration of the anticipation epoch was identical across conditions, ensuring equal measurement precision. The specific duration was chosen to enhance detection of task-related differences in the blood oxygen level-dependent

(BOLD) signal ('activation') (Henson, 2007) and to allow sufficient time for sustained responses to become evident. Safety trials were similar but terminated with the delivery of emotionally neutral reinforcers (see below). Valence was continuously signaled during the anticipation epoch ('countdown') by the background color of the display. Temporal certainty was signaled by the nature of the integer stream. Certain trials always began with the presentation of the number 30. On Uncertain trials, integers were randomly drawn from a near-uniform distribution ranging from 1 to 45 to reinforce the impression that they could be much shorter or longer than Certain trials and to minimize incidental temporal learning ('time-keeping'). To concretely demonstrate the variable duration of Uncertain trials, during scanning, the first three Uncertain trials featured short (8.75 s), medium (15.00 s), and long (28.75 s) anticipation epochs. To mitigate potential confusion and eliminate mnemonic demands, a lower-case 'c' or 'u' was presented at the lower edge of the display throughout the anticipatory epoch. White-noise visual masks (3.2 s) were presented between trials to minimize the persistence of visual reinforcers in iconic memory.

Participants were periodically prompted (following the offset of the white-noise visual mask) to rate the intensity of fear/anxiety experienced a few seconds earlier, during the anticipation period of the prior trial, using a 1 (*minimal*) to 4 (*maximal*) scale and an MRI-compatible response pad (MRA, Washington, PA). Each condition was rated once per scan (16.7% trials). Skin conductance was continuously acquired throughout.

Procedures. Prior to scanning, participants practiced an abbreviated version of the paradigm (without electrical stimulation) until they indicated and staff confirmed understanding. Benign and aversive electrical stimulation levels were individually titrated. *Benign Stimulation.* Participants were asked whether they could "reliably detect" a 20 V stimulus and whether it was "at all unpleasant." If the

participant could not detect the stimulus, the voltage was increased by 4 V and the process repeated. If the participant indicated that the stimulus was unpleasant, the voltage was reduced by 4 V and the process was repeated. The final level chosen served as the benign electrical stimulation during the imaging assessment. *Aversive Stimulation.* Participants received a 100 V stimulus and were asked whether it was "as unpleasant as you are willing to tolerate"—an instruction specifically chosen to maximize anticipatory distress and arousal. If the participant indicated that they were willing to tolerate more intense stimulation, the voltage was increased by 10 V and the process repeated. If the participant indicated that the stimulus was too intense, the voltage was reduced by 5 V and the process repeated. The final level chosen served as the aversive electrical stimulation during the imaging assessment. Following each scan, staff re-assessed whether stimulation was sufficiently intense and increased the level as necessary (for descriptive statistics, see Grogans et al., 2024; Kim et al., 2023).

Electrical Stimuli. Electrical stimuli (100 ms; 2 ms pulses every 10 ms) were generated using an MRI-compatible constant-voltage stimulator system (STMEPM-MRI; Biopac Systems, Inc., Goleta, CA) and delivered using MRI-compatible, disposable carbon electrodes (Biopac) attached to the fourth and fifth digits of the left hand.

Visual Stimuli. Seventy-two aversive and benign photographs (1.8 s) were selected from the International Affective Picture System (for details, see Hur et al., 2020). Visual stimuli were back-projected (Powerlite Pro G5550, Epson America, Inc., Long Beach, CA) onto a semi-opaque screen mounted at the head-end of the scanner bore and viewed using a mirror mounted on the head-coil.

Auditory Stimuli. Seventy-two aversive and benign auditory stimuli (0.8 s) were adapted from open-access online sources and delivered using an amplifier (PA-1 Whirlwind) with in-line noise-reducing filters and ear buds (S14; Sensimetrics, Gloucester, MA) fitted with noise-reducing ear plugs (Hearing Components, Inc., St. Paul, MN).

Skin Conductance. Skin conductance was continuously acquired during each scan using a Biopac system (MP-150; Biopac Systems, Inc., Goleta, CA). Skin conductance (250 Hz; 0.05 Hz high-pass) was measured using MRI-compatible disposable electrodes (EL507) attached to the second and third digits of the left hand.

Data were acquired using a single Siemens Magnetom TIM Trio 3 Tesla scanner (32-channel head-coil). Foam inserts were used to immobilize the participant's head within the head-coil. Participants were continuously monitored using an eye-tracker (Eyelink 1000; SR Research, Ottawa, Ontario, Canada) and the AFNI real-time motion plugin (Cox, 1996). Eye-tracking data were not recorded. Sagittal T1-weighted anatomical images were acquired using a magnetization prepared rapid acquisition gradient echo sequence (TR=2,400 ms; TE=2.01 ms; inversion time=1,060 ms; flip=8°; slice thickness=0.8 mm; in-plane=0.8×0.8 mm; matrix=300×320; field-of-view=240×256). A T2-weighted image was collected co-planar to the T1-weighted image (TR=3,200 ms; TE=564 ms; flip angle=120°). A multi-band sequence was used to collect oblique-axial echo-planar imaging (EPI) volumes (multiband acceleration=6; TR=1,250 ms; TE=39.4 ms; flip=36.4°; slice thickness=2.2 mm, number of slices=60; in-plane resolution=2.1875×2.1875 mm; matrix=96×96). Data were collected in the oblique-axial plane (approximately −20° relative to the AC-PC plane) to minimize susceptibility artifacts. Three 478-volume EPI scans were acquired. The scanner automatically discarded the first 7 volumes. To enable fieldmap correction, two oblique-axial spin echo

(SE) images were collected in opposing phase-encoding directions (rostral-to-caudal and caudal-to-rostral) at the same location and resolution as the functional volumes (i.e., co-planar; TR=7,220 ms; TE=73 ms). Respiration and pulse were continuously acquired during scanning using a respiration belt and photo-plethysmograph affixed to the first digit of the non-dominant hand.

Skin Conductance Data Processing Pipeline

Skin conductance data were processed using *PsPM* (version 4.0.2) and in-house Matlab (version 9.9.0.1467703) code (Bach et al., 2018; Bach & Friston, 2013). Data were orthogonalized with respect to pulse and respiration signals and de-spiked using *filloutliers* (150-sample moving-median widow; modified Akima cubic Hermite interpolation). Each scan was then band-pass filtered (0.009-0.333 Hz), median centered, and down-sampled (4 Hz). Participant-specific skin conductance response functions (SCRFs) were estimated by fitting the four parameters of the canonical SCRF (Bach et al., 2010) to the grand-average reinforcer response using *fmincon* and a cost function that maximized variance explained and penalized negative coefficients.

Skin Conductance Modeling

Robust general linear models (GLMs) were used to separate electrodermal signals associated with threat anticipation from those evoked by other aspects of the task (e.g., reinforcer presentation). Modeling was performed separately for each participant and scan using *robustfit*. Subject-specific SCRFs were convolved with rectangular regressors time-locked to the presentation of the reinforcers (separately for each trial type), visual masks, and rating prompts. The first-level residuals were then averaged separately for each

participant and condition, enabling us to quantify skin conductance level (SCL) during the anticipation ('countdown') epochs.

MRI Pipeline

Methods were optimized to minimize spatial normalization error and other potential sources of noise and are similar to other recent work by our group (Cornwell et al., 2025). Data were visually inspected before and after processing for quality assurance.

Anatomical Data Processing. T1- and T2-weighted images were inhomogeneity corrected using *N4* (Tustison et al., 2010) and denoised using *ANTS* (Avants et al., 2011). The brain was then extracted using a combination of *BEaST* (Eskildsen et al., 2012) and brain-extracted and normalized reference brains from *IXI* (BIAC, 2022). Extracted T1 images were normalized to a variant of the 1-mm T1-weighted MNI152 template that was modified to remove extracerebral tissue (non-linear 6th-generation symmetric average; Grabner et al., 2006). Normalization was performed using the diffeomorphic approach implemented in *SyN* (version 2.3.4) (Avants et al., 2011). T2-weighted images were rigidly co-registered with the corresponding T1 prior to normalization. The brain extraction mask from the T1 was then applied. Tissue priors were unwarped to native space using the inverse diffeomorphic transformation (Lorio et al., 2016). Brain-extracted T1 and T2 images were segmented using native-space priors generated in *FAST* (version 6.0.4) for use in T1-EPI co-registration (Jenkinson et al., 2012).

Fieldmap Data Processing. SE images and *topup* were used to create fieldmaps. Fieldmaps were converted to radians, median-filtered, and smoothed (2-mm). The average of the distortion-corrected SE images was

inhomogeneity corrected using *N4* and masked to remove extracerebral voxels using *3dSkullStrip* (version 19.1.00). The resulting mask was minimally eroded to further exclude extracerebral voxels.

Functional Data Processing. EPI files were de-spiked using *3dDespike*, slice-time corrected to the TR-center using *3dTshift*, and motion-corrected to the first volume and inhomogeneity corrected using *ANTS* (12-parameter affine). Transformations were saved in ITK-compatible format for subsequent processing (McCormick et al., 2014). The first volume was extracted for EPI-T1 co-registration. The reference EPI volume was simultaneously co-registered with the corresponding T1-weighted image in native space and corrected for geometric distortions using boundary-based registration (Jenkinson et al., 2012). This step incorporated the previously created fieldmap, undistorted SE, T1, white matter (WM) image, and masks. The spatial transformations necessary to transform each EPI volume from native space to the reference EPI, from the reference EPI to the T1, and from the T1 to the template were concatenated and applied to the processed EPI data in a single step to minimize incidental spatial blurring. Normalized EPI data were resampled (2 mm^3) using fifth-order b-splines. Voxelwise analyses employed data that were spatially smoothed (4-mm) using *3DblurInMask*. To minimize signal mixing, smoothing was confined to the gray-matter compartment, defined using a variant of the Harvard-Oxford cortical and subcortical atlases that was expanded to include the bed nucleus of the stria terminalis (BST) and periaqueductal gray (PAG) (Desikan et al., 2006; Edlow et al., 2012; Frazier et al., 2005; Makris et al., 2006; Theiss et al., 2017). Focal analyses of the extended amygdala (EA) leveraged spatially unsmoothed data and anatomically defined regions of interest (ROIs; see below), consistent with prior work by our group (Cornwell et al., 2025).

fMRI Data Modeling

First-Level Modeling. For each participant, first-level modeling was performed using GLMs implemented in *SPM12* (version 7771), with the default autoregressive model and the temporal band-pass filter set to the hemodynamic response function (HRF) and 128 s (~0.0078-0.1667 Hz; Wellcome Centre for Human Neuroimaging, 2022). Regressors were convolved with a canonical HRF and its temporal derivative. For the threat-anticipation paradigm, hemodynamic activity was modeled using variable-duration rectangular ('boxcar') regressors that spanned the entirety of the anticipation ('countdown') epochs of the Uncertain-Threat, Certain-Threat, and Uncertain-Safety trials. To maximize design efficiency, Certain-Safety anticipation served as the reference condition and contributed to the implicit baseline estimate. Epochs corresponding to the presentation of the four types of reinforcers, white-noise visual masks, and rating prompts were simultaneously modeled using the same approach. EPI volumes acquired before the first trial and following the final trial were unmodeled and contributed to the baseline estimate. Consistent with prior work (Cornwell et al., 2025), nuisance variates included volume-to-volume displacement and first derivative, 6 motion parameters and first derivatives, cerebrospinal fluid (CSF) signal, instantaneous pulse and respiration rates, and nuisance signals (e.g., brain edge, CSF edge, global motion, WM, and extracerebral soft tissue) (Anderson et al., 2011; Pruim et al., 2015). Volumes with excessive volume-to-volume displacement (>0.5 mm) and those during and immediately following reinforcer delivery were censored. On average, 3.39 volumes were censored per run (*SD*=4.42).

Anatomical ROIs. Ce and BST activation was quantified using well-established, anatomically defined regions-of-interest (ROIs) and spatially unsmoothed data (Theiss et al., 2017; Tillman et al., 2018). The BST ROI mostly encompasses the supra-commissural BST, given the difficulty of reliably discriminating the sub-commissural BST border in standard anatomical images (Kruger et al., 2015; Walter et al., 1991). Bilateral ROIs were decimated to the 2-mm resolution of the fMRI data. ROI analyses used standardized regression coefficients extracted and averaged for each combination of task contrast (e.g., Uncertain-Threat

anticipation vs. Uncertain-Safety anticipation), region, and participant. Anatomical ROIs enable statistically unbiased tests of regional sensitivity to specific experimental manipulations (i.e., Region × Condition effects), including potential single and double dissociations (e.g., BST: Uncertain > Certain Threat; Ce: Uncertain < Certain Threat) (Fox et al., 2018; Poldrack et al., 2017).

Analytic Strategy

Overview. Except where noted otherwise, analyses were performed using *SPM12* (version 7771) and *SPSS* (version 27.0.1.0) (Wellcome Centre for Human Neuroimaging, 2022). Diagnostic procedures and data visualizations were used to confirm that test assumptions were satisfied (Tukey, 1977). Standardized frequentist (Cohen's *d*) effect sizes were interpreted using established benchmarks (Cohen, 1988; Cohen, 1994; Schimmack, 2019), ranging from *large* (*d*=0.80), to *medium* (*d*=0.50), to *small* (*d*=0.20), to *nil* (*d*≤0.10). Some figures were created using created using *ggplot2* (version 3.3.6) (Wickham, 2016) and *MRIcron* (Rorden, 2019). Clusters and local maxima were labeled using the Harvard–Oxford atlas (Desikan et al., 2006; Frazier et al., 2005; Makris et al., 2006), supplemented by other resources (ten Donkelaar et al., 2018).

JASP (version 0.16.4.0) was used to compute Bayesian effect sizes for select analyses (Love et al., 2019; van Doorn et al., 2021). Here, Bayes Factor (BF_{10}) quantifies the relative performance of the null hypothesis (H_0; e.g., the absence of a credible mean difference) and the alternative hypothesis (H_1; e.g., the presence of a credible mean difference), on a 0 to ∞ scale. A key advantage of *BF* is that it can be used to quantify the relative strength of the evidence for H_0 (test the null), unlike conventional frequentist null-hypothesis significance tests (Bo et al., 2024; Wagenmakers et al., 2018). It also does not require the data analyst to

arbitrarily decide what constitutes a 'statistically indistinguishable' difference, in contrast to traditional equivalence tests (Hur et al., 2020). The Bayesian approach provides readily interpretable, principled effect-size benchmarks (van Doorn et al., 2021). Values >1 were interpreted as evidence of mean differences in activation across conditions, ranging from *strong* (BF_{10}>10), to *moderate* (BF_{10}=3-10), to *weak* (BF_{10}=1-3). Values <1 were interpreted as evidence of statistical equivalence (i.e., support for the null hypothesis), ranging from s*trong* (BF_{10}<0.10), to *moderate* (BF_{10}=0.10-0.33), to *weak* (BF_{10}=0.33-1). The reciprocal of BF_{10} represents the relative likelihood of the null hypothesis (e.g., BF_{10}=0.10, H_0 is 10 times more likely than H_1). Bayesian effects were computed using a noninformative zero-centered Cauchy distribution ($\omega=1/\sqrt{2}$), the default setting in *JASP* and the field standard for two-sided tests (Gronau et al., 2020; Schmalz et al., 2023; Schönbrodt et al., 2017; van Doorn et al., 2021; Wagenmakers et al., 2018). Across tests, the estimated error of the MCMC-derived (Markov Chain Monte Carlo) BF_{10} estimates was negligible (<0.30%) and stable across a range of priors.

Ratings and Psychophysiology. We used repeated-measures general linear models (GLMs) to confirm that the threat-anticipation paradigm amplified subjective symptoms of distress (in-scanner fear/anxiety ratings) and objective signs of arousal (SCL). Interactions were probed using focal contrasts. Sensitivity analyses confirmed that none of the conclusions materially changed when controlling for potential nuisance variation in mean-centered study, age, and assigned sex (for additional details, see the study OSF collection).

Whole-Brain Voxelwise Tests. Spatially smoothed (4-mm) data and whole-brain voxelwise ('second-level') repeated-measures GLMs ('random effects') were used to compare each threat-anticipation condition to its corresponding control condition (e.g., Uncertain-Threat vs. Uncertain-Safety anticipation),

while accounting for potential nuisance variation in mean-centered dummy-coded study (Grogans et al., 2024; Kim et al., 2023), age, and assigned sex. Significance was assessed using $p<0.05$ (whole-brain familywise error [FWE] corrected). A minimum-conjunction test (logical 'AND') was used to identify the subset of voxels significantly sensitive to both Certain- *and* Uncertain-Threat anticipation (Nichols et al., 2005). We also directly examined potential differences in anticipatory activity between the two threat conditions (Certain Threat vs. Uncertain Threat). We did not examine hemodynamic responses to reinforcer presentation given the possibility of artifact.

Anatomical ROIs. As a precursor to hypothesis testing, a series of one-sample Student's *t*-tests was used to confirm that the EA (BST/Ce) ROIs—which leveraged spatially unsmoothed data—showed nominally significant recruitment during Certain and Uncertain Threat anticipation relative to their respective control conditions ($p<0.05$, uncorrected). For hypothesis testing, we used a standard 2 (*Region:* Ce, BST) × 2 (*Threat-Certainty:* Certain, Uncertain) repeated-measures GLM to test potential regional differences in activation during the anticipation of temporally Certain Threat (relative to Certain Safety) versus Uncertain Threat (relative to Uncertain Safety). These analyses leveraged spatially unsmoothed data to maximize anatomical resolution and inferential clarity. Interactions were probed using focal contrasts. Sensitivity analyses confirmed that none of the conclusions materially changed when controlling for potential nuisance variation in mean-centered study, age, and assigned sex (for additional details, see the study OSF collection). A sign test (Z_{Sign}) was used to nonparametrically test the proportion of participants showing double dissociations.

Continued…

SUPPLEMENTARY RESULTS

Supplementary Figure S2. ***The BST and Ce show statistically indistinguishable responses to threat.*** **(A)** ***BST.*** The raincloud plot depicts BST reactivity to Certain and Uncertain Threat. Ring plot indicates the percentage of participants showing greater BST activation during Certain versus Uncertain threat anticipation. **(B)** ***Ce.*** The raincloud plot depicts BST reactivity to Certain and Uncertain Threat. Ring plot indicates the percentage of participants showing greater Ce activation during Certain versus Uncertain threat anticipation. Raincloud plots depict the median (*horizontal lines*), interquartile range (*boxes*), individual participants (*dots*), and smoothed data distributions (*half violins*) for each contrast. Whiskers indicate 1.5× the interquartile range. Gray lines depict the sign and magnitude of intra-individual mean differences. Abbreviations—BF, Bayes Factor; BST, bed nucleus of the stria terminalis; Ce, central nucleus of the amygdala; *d*, Cohen's *d*. **(C)** ***Testing regional differences.*** The raincloud plot depicts the Region × Condition interaction as a 1-*df* contrast ('difference of differences'). Ring plot indicates the percentage of participants showing the RDoC-hypothesized dissociation of regional reactivity to threat (BST: Certain < Uncertain Threat; Ce: Certain > Uncertain Threat).

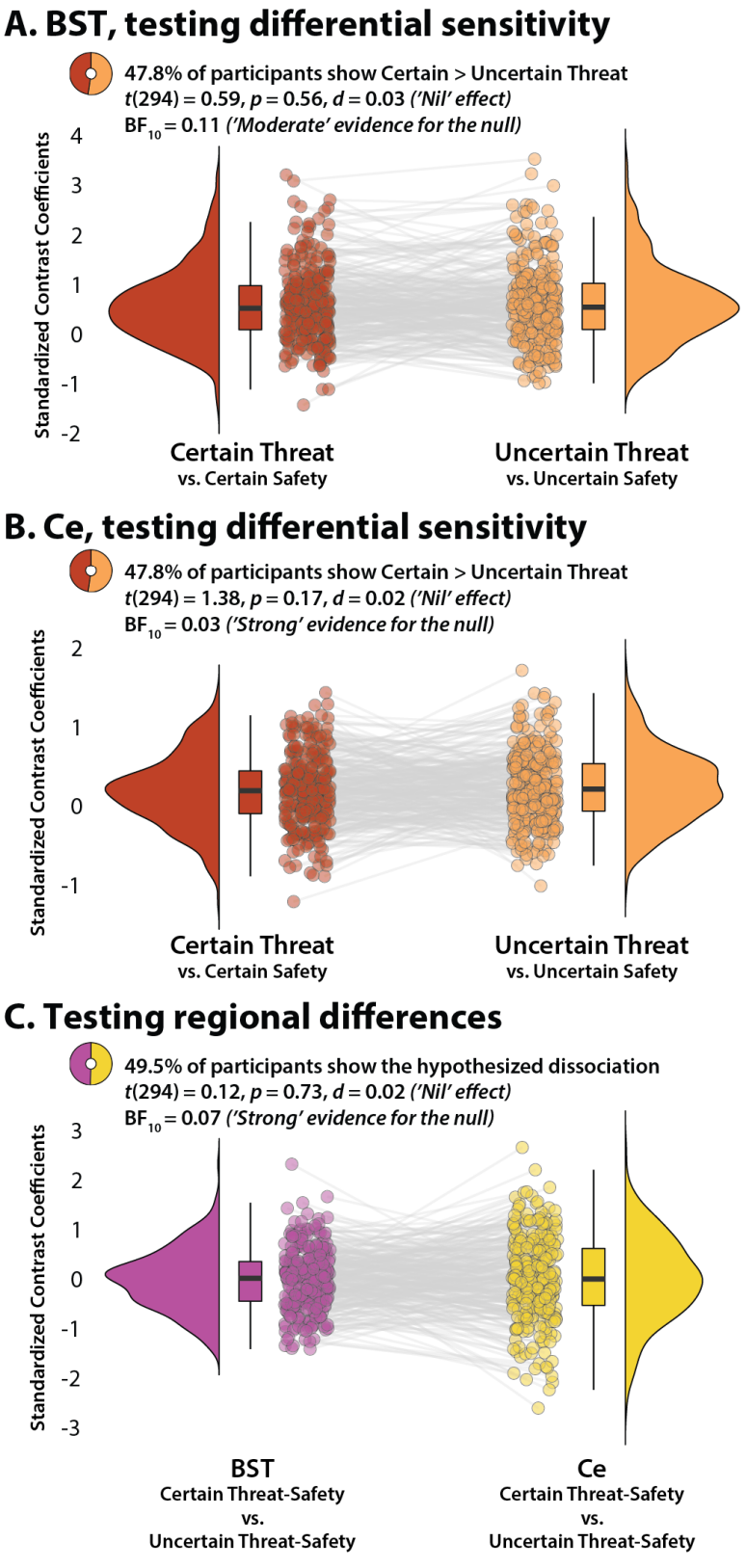

SUPPLEMENTARY TABLES

Supplementary Table S1. Descriptive statistics for clusters and local extrema showing greater activation during the anticipation of Uncertain Threat relative to Uncertain Safety (FWE $p<0.05$, whole-brain corrected, 4-mm smoothing kernel).

		mm³	***t***	**x**	**y**	**z**
	Cluster 1	516,112				
	L Frontal Operculum Cortex		21.66	-40	14	2
	L Insular Cortex		20.23	-32	24	6
	L Cingulate Gyrus, anterior division		19.08	-6	10	40
	L Paracingulate Gyrus		18.97	-8	12	38
	L Temporal Occipital Fusiform Cortex		18.48	-28	-60	-18
	L Brain Stem		16.62	-2	-28	-2
	L Left Putamen		16.13	-22	8	-4
	L Central Opercular Cortex		15.88	-52	4	2
	L Supramarginal Gyrus, anterior division		15.38	-64	-32	22
	L Superior Frontal Gyrus		15.32	-14	2	70
	L Cingulate Gyrus, posterior division		15.25	-10	-22	40
	L Supramarginal Gyrus, posterior division		15.12	-58	-50	34
	L Precentral Gyrus		15.11	-40	-4	48
	L Middle Frontal Gyrus		14.70	-40	-2	58
	L Thalamus		14.55	-10	-6	14
	L Juxtapositional Lobule Cortex		14.53	-8	2	52
	L Caudate		14.39	-10	0	10
	L Parietal Operculum Cortex		12.56	-62	-26	18
	L Superior Parietal Lobule		11.84	-20	-50	64
	L Precuneus Cortex		11.64	-10	-48	52
	L Postcentral Gyrus		11.22	-58	-22	24
	L Inferior Frontal Gyrus, pars opercularis		11.12	-58	10	18
	L Middle Temporal Gyrus, temporooccipital part		10.57	-46	-60	10

	L Lateral Occipital Cortex, inferior division		10.04	-54	-66	10
	L Lingual Gyrus		9.94	-12	-86	-12
	L Occipital Pole		9.26	-20	-96	12
	L Lateral Occipital Cortex, superior division		9.03	-32	-60	58
	L Angular Gyrus		8.97	-48	-54	52
	L Pallidum		7.60	-26	-14	-2
	L Planum Polare		7.35	-42	-2	-14
	L Temporal Fusiform Cortex, posterior division		6.50	-44	-40	-22
	L Temporal Pole		5.87	-46	18	-22
	R Paracingulate Gyrus		20.98	8	20	36
	R Frontal Orbital Cortex		20.70	34	28	2
	R Frontal Operculum Cortex		19.68	36	22	8
	R Central Opercular Cortex		18.92	48	6	0
	R Juxtapositional Lobule Cortex		18.84	6	6	48
	R Putamen		18.23	22	6	-6
	R Cingulate Gyrus, anterior division		18.09	10	6	42
	R Precentral Gyrus		18.04	44	-2	48
	R Supramarginal Gyrus, posterior division		17.55	62	-42	22
	R Brain Stem		17.44	4	-30	-2
	R Superior Frontal Gyrus		17.16	2	10	56
	R Caudate		17.06	12	-2	14
	R Inferior Frontal Gyrus, pars triangularis		16.12	56	22	0
	R Cingulate Gyrus, posterior division		15.85	10	-22	42
	R Parietal Operculum Cortex		15.71	56	-28	26
	R Frontal Pole		15.62	32	48	28
	R Middle Frontal Gyrus		14.95	50	8	42
	R Temporal Occipital Fusiform Cortex		14.92	32	-54	-20
	R Superior Parietal Lobule		14.40	24	-46	66
	R Middle Temporal Gyrus, posterior division		13.51	50	-24	-6

	R Angular Gyrus		12.85	58	-50	42
	R Thalamus		12.81	6	-20	-2
	R Postcentral Gyrus		12.03	32	-38	62
	R Inferior Frontal Gyrus, pars opercularis		11.81	40	16	26
	R Precuneus Cortex		11.27	8	-54	56
	R Middle Temporal Gyrus, temporooccipital part		11.23	54	-60	6
	R Occipital Pole		11.13	22	-96	16
	R Lingual Gyrus		9.26	10	-80	-6
	R Planum Polare		9.15	42	-4	-12
	R Amygdala		9.14	28	-10	-12
	R Occipital Fusiform Gyrus		8.91	22	-80	-12
	R Lateral Occipital Cortex, inferior division		8.83	42	-78	-10
	R Lateral Occipital Cortex, superior division		8.58	16	-80	40
	R Insular Cortex		8.33	40	-16	-2
	R Pallidum		7.30	14	-4	-4
	R Inferior Temporal Gyrus, temporooccipital part		7.25	48	-54	-14
	R Heschls Gyrus (includes H1 and H2)		6.53	44	-12	4
	Cluster 2	15,144				
	L Frontal Pole		16.21	-28	48	26
	L Middle Frontal Gyrus		14.75	-34	36	40
	Cluster 3	1,672				
	R Temporal Pole		6.08	46	12	-42
	Cluster 4	688				
	L Middle Temporal Gyrus, posterior division		6.27	-60	-28	-2
	Cluster 5	376				
	R Frontal Pole		7.49	26	50	-14
	Cluster 6	320				
	L Temporal Pole		6.89	-40	6	-38
	Cluster 7	272				

	L Middle Temporal Gyrus, anterior division		6.50	-50	-2	-30
	Cluster 8	216				
	R Occipital Pole		6.74	6	-96	-8
	Cluster 9	176				
	R Temporal Pole		6.72	52	8	-20
	Cluster 10	144				
	R Parahippocampal Gyrus, anterior division		6.19	24	-8	-32
	Cluster 11	104				
	L Amygdala		7.67	-26	-12	-12
	Cluster 12	80				
	L Frontal Pole		6.38	-30	54	-14
	Cluster 13	64				
	L Parahippocampal Gyrus, anterior division		5.89	-24	-6	-32
	Cluster 14	24				
	L Temporal Fusiform Cortex, anterior division		5.22	-36	-2	-42
	Cluster 15	24				
	L Frontal Pole		5.67	-26	46	-14
	Cluster 16	24				
	R Frontal Pole		5.55	30	66	0
	Cluster 17	16				
	L Parahippocampal Gyrus, anterior division		5.58	-24	-10	-38
	Cluster 18	16				
	R Amygdala		5.53	18	-14	-12
	Cluster 19	8				
	L Temporal Pole		5.24	-20	2	-40
	Cluster 20	8				
	R Brain Stem		5.70	8	-24	-34
	Cluster 21	8				
	R Hippocampus		5.44	12	-12	-20

	Cluster 22	8				
	L Frontal Pole		5.14	-24	50	-14
	Cluster 23	8				
	R Frontal Pole		5.13	22	62	-8
	Cluster 24	8				
	R Hippocampus		5.15	34	-28	-6
	Cluster 25	8				
	L Frontal Pole		5.34	-26	66	-4
	Cluster 26	8				
	L Hippocampus		5.20	-20	-38	-2
	Cluster 27	8				
	R Frontal Pole		5.36	14	64	26
	Cluster 28	8				
	R Postcentral Gyrus		5.42	22	-30	62

Note: Suprathreshold activation was also evident in the bilateral periaqueductal gray, bilateral bed nucleus of the stria terminalis, and bilateral dorsal amygdala.

Supplementary Table S2. Descriptive statistics for clusters and local extrema showing greater activation during the anticipation of Uncertain Safety relative to Uncertain Threat (FWE $p<0.05$, whole-brain corrected, 4-mm smoothing kernel).

		mm^3	*t*	x	y	z
	Cluster 1	30,088				
	L Intracalcarine Cortex		19.11	-14	-80	6
	L Cingulate Gyrus, posterior division		10.74	-4	-50	14
	L Lingual Gyrus		10.55	-10	-60	4
	L Precuneus Cortex		10.40	-10	-62	18
	R Intracalcarine Cortex		18.87	14	-78	10
	R Precuneus Cortex		14.57	2	-68	22
	R Supracalcarine Cortex		13.91	2	-66	18
	R Cingulate Gyrus, posterior division		10.39	10	-50	4
	Cluster 2	5,000				
	L Postcentral Gyrus		11.41	-52	-10	26
	Cluster 3	3,640				
	L Precentral Gyrus		8.43	-6	-24	60
	L Postcentral Gyrus		6.85	-10	-40	70
	R Precentral Gyrus		10.41	2	-32	66
	Cluster 4	3,112				
	R Precentral Gyrus		11.07	54	-6	26
	R Postcentral Gyrus		9.93	64	-6	34
	Cluster 5	2,600				
	L Frontal Medial Cortex		5.73	-6	54	-12
	R Frontal Pole		9.58	0	64	-10
	R Frontal Medial Cortex		8.36	2	52	-12
	R Subcallosal Cortex		5.49	4	28	-18
	Cluster 6	1,568				
	L Lateral Occipital Cortex, superior division		7.85	-38	-84	38

	Cluster 7	1,328				
	R Lateral Occipital Cortex, superior division		7.61	50	-72	36
	Cluster 8	1,016				
	L Insular Cortex		10.02	-38	-12	14
	L Central Opercular Cortex		7.88	-44	-12	18
	Cluster 9	872				
	R Insular Cortex		10.33	38	-8	12
	R Central Opercular Cortex		7.57	46	-10	16
	Cluster 10	576				
	R Parahippocampal Gyrus, posterior division		7.93	28	-32	-18
	R Lingual Gyrus		6.21	26	-40	-10
	Cluster 11	568				
	L Parahippocampal Gyrus, posterior division		7.43	-28	-38	-14
	L Temporal Fusiform Cortex, posterior division		6.31	-32	-32	-18
	Cluster 12	328				
	R Precentral Gyrus		6.19	14	-28	66
	Cluster 13	248				
	R Hippocampus		7.49	22	-18	-20
	R Amygdala		5.51	18	-8	-18
	Cluster 14	184				
	L Hippocampus		7.83	-18	-16	-22
	Cluster 15	112				
	R Postcentral Gyrus		6.93	12	-40	70
	Cluster 16	88				
	L Cingulate Gyrus, posterior division		5.62	-6	-38	34
	Cluster 17	88				
	L Precentral Gyrus		6.61	-12	-28	72
	Cluster 18	80				
	R Frontal Pole		5.91	38	36	-12

	Cluster 19	56				
	L Middle Temporal Gyrus, anterior division		5.94	-64	-4	-18
	Cluster 20	56				
	R Superior Frontal Gyrus		5.32	20	30	46
	Cluster 21	24				
	L Hippocampus		5.48	-22	-20	-16
	Cluster 22	24				
	L Frontal Orbital Cortex		5.59	-34	36	-10
	Cluster 23	24				
	R Lingual Gyrus		5.38	18	-46	-8
	Cluster 24	24				
	R Subcallosal Cortex		5.79	2	14	-6
	Cluster 25	16				
	R Middle Temporal Gyrus, anterior division		5.55	64	0	-20
	Cluster 26	16				
	L Precentral Gyrus		5.18	-12	-26	78
	Cluster 27	8				
	R Subcallosal Cortex		5.21	2	22	-24
	Cluster 28	8				
	R Subcallosal Cortex		5.19	0	26	-24
	Cluster 29	8				
	L Amygdala		5.32	-30	2	-18
	Cluster 30	8				
	L Hippocampus		5.38	-28	-18	-16
	Cluster 31	8				
	L Frontal Orbital Cortex		5.11	-40	36	-14
	Cluster 32	8				
	L Frontal Medial Cortex		5.11	-6	48	-14
	Cluster 33	8				

	L Frontal Medial Cortex		5.19	-8	52	-10
	Cluster 34	8				
	R Hippocampus		5.72	24	-26	-8
	Cluster 35	8				
	R Cuneal Cortex		5.12	0	-86	34

Supplementary Table S3. Descriptive statistics for clusters and local extrema showing greater activation during the anticipation of Certain Threat relative to Certain Safety (FWE $p<0.05$, whole-brain corrected).

		mm³	***t***	**x**	**y**	**z**
	Cluster 1	448,752				
	L Superior Frontal Gyrus		15.05	-14	-2	68
	L Frontal Operculum Cortex		14.25	-34	16	10
	L Putamen		13.61	-22	14	-6
	L Cingulate Gyrus, anterior division		13.34	-8	18	34
	L Juxtapositional Lobule Cortex		13.24	-4	4	56
	L Thalamus		13.19	-10	-6	14
	L Bed Nucleus of the Stria Terminalis		12.97	-6	4	0
	L Supramarginal Gyrus, posterior division		12.80	-58	-50	40
	L Paracingulate Gyrus		12.72	-8	22	32
	L Lateral Occipital Cortex, superior division		12.56	-36	-58	58
	L Middle Frontal Gyrus		12.05	-34	-4	64
	L Insular Cortex		11.78	-32	26	4
	L Superior Parietal Lobule		11.68	-34	-58	52
	L Occipital Fusiform Gyrus		11.61	-30	-72	-20
	L Brain Stem		11.52	-2	-28	-4
	L Frontal Pole		11.51	-30	52	28
	L Lingual Gyrus		11.30	-4	-74	-12
	L Central Opercular Cortex		11.20	-44	4	2
	L Caudate		10.65	-14	18	-4

	L Precentral Gyrus		10.62	-40	-2	46
	L Frontal Orbital Cortex		10.50	-32	26	-6
	L Inferior Frontal Gyrus, pars triangularis		10.16	-44	22	8
	L Angular Gyrus		9.90	-50	-56	48
	L Parietal Operculum Cortex		9.77	-60	-38	24
	L Precuneus Cortex		9.49	-10	-78	36
	L Cingulate Gyrus, posterior division		9.31	-2	-26	28
	L Supramarginal Gyrus, anterior division		8.34	-60	-38	46
	L Postcentral Gyrus		8.30	-20	-32	76
	L Accumbens		7.92	-8	12	-6
	L Inferior Frontal Gyrus, pars opercularis		7.69	-54	10	16
	L Middle Temporal Gyrus, temporooccipital part		7.01	-62	-56	6
	L Lateral Occipital Cortex, inferior division		6.25	-56	-64	10
	L Temporal Pole		6.12	-50	18	-18
	L Hippocampus		5.64	-30	-12	-16
	L Periaqueductal Gray		5.52	-2	-34	-12
	L Superior Temporal Gyrus, posterior division		5.30	-66	-38	6
	R Putamen		15.93	22	10	-8
	R Superior Frontal Gyrus		15.64	20	-8	70
	R Paracingulate Gyrus		15.16	8	20	36
	R Caudate		14.92	12	-4	16
	R Precentral Gyrus		14.52	46	0	50
	R Juxtapositional Lobule Cortex		14.08	2	6	48
	R Bed Nucleus of the Stria Terminalis		13.93	8	4	2
	R Postcentral Gyrus		13.84	34	-36	62
	R Thalamus		13.41	10	-2	12
	R Frontal Pole		13.02	30	44	24
	R Superior Parietal Lobule		12.93	24	-44	66
	R Frontal Operculum Cortex		12.55	34	24	8

	R Supramarginal Gyrus, posterior division		12.54	62	-38	32
	R Middle Frontal Gyrus		12.45	38	-2	50
	R Angular Gyrus		12.29	62	-46	30
	R Central Opercular Cortex		11.69	52	6	2
	R Lateral Occipital Cortex, superior division		11.46	28	-58	62
	R Brain Stem		10.80	4	-28	-2
	R Superior Temporal Gyrus, posterior division		10.67	48	-26	-4
	R Cingulate Gyrus, anterior division		10.16	0	10	34
	R Precuneus Cortex		10.01	8	-56	56
	R Frontal Orbital Cortex		9.63	40	20	-8
	R Cingulate Gyrus, posterior division		9.54	10	-24	42
	R Accumbens		9.49	10	12	-4
	R Parietal Operculum Cortex		9.06	56	-28	26
	R Inferior Frontal Gyrus, pars triangularis		8.66	54	28	-6
	R Supramarginal Gyrus, anterior division		8.36	60	-24	28
	R Middle Temporal Gyrus, posterior division		8.32	54	-22	-10
	R Amygdala		8.32	30	-10	-14
	R Inferior Frontal Gyrus, pars opercularis		7.95	46	12	28
	R Lateral Occipital Cortex, inferior division		7.74	42	-84	-8
	R Middle Temporal Gyrus, temporooccipital part		7.32	60	-60	6
	R Insular Cortex		6.99	40	10	-8
	R Planum Polare		6.26	42	-4	-14
	R Occipital Pole		5.88	26	-94	18
	R Pallidum		5.47	16	-4	-4
	R Periaqueductal Gray		5.40	2	-36	-12
	R Temporal Occipital Fusiform Cortex		5.30	44	-54	-16
	Cluster 2	792				
	L Brain Stem		6.73	-8	-38	-46
	R Brain Stem		8.04	2	-34	-48

	Cluster 3	776				
	L Lateral Occipital Cortex, inferior division		7.00	-40	-82	-6
	L Occipital Pole		5.50	-36	-92	-8
	Cluster 4					
	Middle Temporal Gyrus, posterior division		6.95	-66	-24	-6
	Superior Temporal Gyrus, posterior division		6.71	-60	-26	-2
	Cluster 5	224				
	R Temporal Pole		6.31	42	6	-38
	R Middle Temporal Gyrus, anterior division		6.29	48	0	-32
	Cluster 6	224				
	L Frontal Pole		6.05	-32	48	-14
	Cluster 7	168				
	L Occipital Pole		5.82	-22	-96	12
	Cluster 8	168				
	R Precentral Gyrus		6.85	6	-30	76
	Cluster 9	152				
	R Frontal Pole		6.34	40	46	6
	Cluster 10	96				
	L Hippocampus		6.17	-22	-36	-4
	Cluster 11					
	L Planum Polare		6.74	-42	-4	-14
	L Insular Cortex		6.58	-40	-2	-16
	Cluster 12	88				
	R Frontal Pole		6.05	26	48	-14
	Cluster 13	80				
	R Brain Stem		5.97	18	-34	-28
	Cluster 14	72				
	L Lateral Occipital Cortex, inferior division		5.73	-48	-64	4
	Cluster 15	72				

	L Middle Temporal Gyrus, temporooccipital part		6.13	-46	-58	10
	Cluster 16	64				
	L Brain Stem		6.46	-6	-46	-56
	Cluster 17	64				
	R Brain Stem		5.58	0	-36	-38
	Cluster 18	64				
	L Brain Stem		6.95	-4	-34	-24
	Cluster 19	48				
	L Brain Stem		6.79	-12	-24	-20
	Cluster 20	48				
	L Lateral Occipital Cortex, inferior division		5.54	-50	-74	-10
	Cluster 21	40				
	L Brain Stem		5.71	-8	-38	-30
	Cluster 22	40				
	L Brain Stem		5.71	-8	-20	-22
	Cluster 23	32				
	L Brain Stem		6.15	-4	-18	-20
	Cluster 24	32				
	R Inferior Temporal Gyrus, temporooccipital part		5.86	60	-58	-18
	Cluster 25	32				
	R Inferior Temporal Gyrus, temporooccipital part		5.50	60	-58	-12
	Cluster 26	32				
	R Lateral Occipital Cortex, inferior division		5.44	44	-72	-4
	Cluster 27	32				
	R Hippocampus		5.63	20	-36	6
	Cluster 28	32				
	R Central Opercular Cortex		5.32	48	-18	14
	Cluster 29	16				
	R Hippocampus		5.95	16	-12	-16

	Cluster 30	16				
	R Cingulate Gyrus, posterior division		5.44	4	-38	24
	Cluster 31	16				
	L Middle Frontal Gyrus		5.24	-50	22	30
	Cluster 32	8				
	R Brain Stem		5.20	8	-36	-28
	Cluster 33	8				
	R Brain Stem		5.25	6	-34	-26
	Cluster 34	8				
	L Middle Temporal Gyrus, posterior division		5.17	-54	-30	-6
	Cluster 35	8				
	L Pallidum		5.25	-20	-10	-4
	Cluster 36	8				
	L Frontal Pole		5.26	-50	42	0
	Cluster 37	8				
	R Frontal Pole		5.98	30	68	2
	Cluster 38	8				
	L Lateral Occipital Cortex, inferior division		5.43	-54	-70	6
	Cluster 39	8				
	L Lateral Occipital Cortex, inferior division		5.52	-42	-72	10
	Cluster 40	8				
	R Lateral Occipital Cortex, inferior division		6.02	42	-68	10
	Cluster 41	8				
	R Lateral Occipital Cortex, inferior division		5.24	42	-62	12
	Cluster 42	8				
	R Parietal Operculum Cortex		5.20	46	-22	16
	Cluster 43	8				
	R Occipital Pole		5.22	18	-98	18
	Cluster 44	8				

	L Angular Gyrus		5.35	-58	-60	18
	Cluster 45	8				
	R Inferior Frontal Gyrus, pars triangularis		5.40	50	26	18
	Cluster 46	8				
	R Lateral Occipital Cortex, superior division		5.26	26	-84	36

Note: Suprathreshold activation was also evident in the bilateral dorsal amygdala.

Supplementary Table S4. Descriptive statistics for clusters and local extrema showing greater activation during the anticipation of Certain Safety relative to Certain Threat (FWE $p<0.05$, whole-brain corrected, 4-mm smoothing kernel).

		mm³	***t***	**x**	**y**	**z**
	Cluster 1	35,472				
	L Intracalcarine Cortex		19.18	-10	-76	10
	L Lingual Gyrus		10.42	-20	-44	-10
	L Precuneus Cortex		8.68	-6	-60	12
	L Occipital Pole		8.46	-10	-98	-4
	L Parahippocampal Gyrus, posterior division		7.48	-30	-34	-16
	L Cingulate Gyrus, posterior division		6.42	-4	-48	14
	R Intracalcarine Cortex		20.15	14	-82	4
	R Lingual Gyrus		17.44	0	-74	6
	R Occipital Pole		15.03	6	-90	6
	R Precuneus Cortex		13.09	0	-68	18
	R Parahippocampal Gyrus, posterior division		8.09	20	-34	-16
	R Occipital Fusiform Gyrus		8.01	28	-68	-6
	R Cingulate Gyrus, posterior division		7.98	10	-50	6
	R Temporal Fusiform Cortex, posterior division		7.67	30	-34	-18
	Cluster 2	288				
	L Postcentral Gyrus		6.49	-62	-8	22
	Cluster 3	272				

	L Subcallosal Cortex		6.25	-2	16	-6
	R Subcallosal Cortex		7.09	2	14	-10
	Cluster 4	168				
	R Frontal Medial Cortex		5.70	2	44	-14
	Cluster 5	160				
	L Lingual Gyrus		6.47	-28	-58	-6
	Cluster 6	40				
	R Frontal Medial Cortex		5.48	0	50	-14
	Cluster 7	32				
	L Temporal Pole		5.58	-42	12	-18
	Cluster 8	32				
	R Subcallosal Cortex		5.56	0	30	-16
	Cluster 9	32				
	R Precentral Gyrus		5.34	56	-6	24
	Cluster 10	24				
	R Parahippocampal Gyrus, anterior division		5.94	20	-20	-22
	Cluster 11	16				
	L Frontal Medial Cortex		5.54	-2	36	-18
	Cluster 12	16				
	R Right Hippocampus		6.65	24	-26	-8
	Cluster 13	16				
	R Precentral Gyrus		5.39	60	-4	28
	Cluster 14	8				
	L Middle Temporal Gyrus, anterior division		5.29	-56	-6	-16
	Cluster 15	8				
	L Frontal Medial Cortex		5.16	-8	42	-14
	Cluster 16	8				
	L Frontal Pole		5.15	-4	56	-12
	Cluster 17	8				

	R Postcentral Gyrus		5.44	66	-6	22

Supplementary Table S5. Descriptive statistics for clusters and local extrema showing greater activation during the anticipation of Uncertain Threat relative to Certain Threat (FWE $p<0.05$, whole-brain corrected).

		mm^3	***t***	**x**	**y**	**z**
	Cluster 1	142,448				
	L Occipital Pole		13.58	-12	-94	-8
	L Temporal Occipital Fusiform Cortex		11.63	-24	-54	-16
	L Occipital Fusiform Gyrus		11.36	-20	-86	-10
	L Cingulate Gyrus, anterior division		9.84	-6	8	40
	L Lateral Occipital Cortex, inferior division		9.30	-32	-86	-18
	L Superior Frontal Gyrus		8.75	-14	10	66
	L Paracingulate Gyrus		8.64	-6	28	30
	L Temporal Fusiform Cortex, posterior division		5.82	-42	-40	-24
	R Occipital Fusiform Gyrus		15.81	30	-78	-10
	R Frontal Orbital Cortex		15.80	34	28	2
	R Frontal Operculum Cortex		15.11	42	24	4
	R Occipital Pole		14.00	26	-94	12
	R Precentral Gyrus		13.40	42	-2	52
	R Lateral Occipital Cortex, inferior division		13.31	44	-80	-10
	R Central Opercular Cortex		12.41	56	4	4
	R Temporal Occipital Fusiform Cortex		12.37	36	-46	-18
	R Middle Frontal Gyrus		12.06	42	0	60
	R Inferior Frontal Gyrus, pars triangularis		12.02	54	22	2
	R Parietal Operculum Cortex		12.00	54	-28	26
	R Juxtapositional Lobule Cortex		11.96	4	4	46
	R Supramarginal Gyrus, anterior division		11.81	60	-26	24
	R Cingulate Gyrus, anterior division		11.78	8	6	42

	R Paracingulate Gyrus		11.62	2	18	38
	R Superior Frontal Gyrus		10.58	4	20	58
	R Inferior Frontal Gyrus, pars opercularis		10.43	60	12	8
	R Supramarginal Gyrus, posterior division		10.37	58	-44	30
	R Putamen		10.28	28	2	-6
	R Cingulate Gyrus, posterior division		10.02	12	-22	42
	R Angular Gyrus		9.92	62	-48	34
	R Middle Temporal Gyrus, temporooccipital part		8.46	46	-56	6
	R Inferior Temporal Gyrus, temporooccipital part		6.80	46	-42	-16
	R Planum Polare		6.49	40	-18	-2
	R Frontal Pole		6.14	54	38	-8
	R Insular Cortex		5.73	38	-14	4
	R Pallidum		5.49	16	2	0
	R Middle Temporal Gyrus, posterior division		5.36	56	-34	0
	Cluster 2	13,728				
	L Insular Cortex		16.18	-32	24	6
	L Frontal Operculum Cortex		14.44	-44	20	-4
	L Inferior Frontal Gyrus, pars opercularis		10.78	-50	20	4
	L Central Opercular Cortex		10.68	-56	2	4
	L Precentral Gyrus		8.83	-56	8	2
	Cluster 3	4,056				
	L Supramarginal Gyrus, posterior division		8.05	-60	-50	44
	L Supramarginal Gyrus, anterior division		8.04	-64	-32	22
	L Parietal Operculum Cortex		7.77	-62	-30	20
	L Angular Gyrus		7.19	-60	-54	38
	Cluster 4	2,272				
	R Superior Parietal Lobule		10.02	22	-46	66
	R Postcentral Gyrus		6.80	34	-38	62
	Cluster 5	1,280				

	L Frontal Pole		7.03	-38	46	30
	Cluster 6	1,232				
	L Brain Stem		6.84	-2	-30	-2
	R Brain Stem		9.53	4	-30	-2
	R Thalamus		7.70	6	-22	-2
	Cluster 7	1,032				
	R Thalamus		7.98	10	0	8
	R Caudate		6.20	16	-10	20
	Cluster 8	776				
	R Frontal Pole		6.68	32	50	26
	Cluster 9	744				
	L Putamen		8.43	-26	6	-8
	L Insular Cortex		6.78	-36	-2	-6
	Cluster 10	680				
	L Precentral Gyrus		7.07	-36	-4	48
	L Middle Frontal Gyrus		6.44	-38	-2	56
	Cluster 11	608				
	R Middle Temporal Gyrus, posterior division		7.23	52	-22	-6
	Cluster 12	552				
	L Cingulate Gyrus, posterior division		6.42	-2	-16	28
	R Cingulate Gyrus, posterior division		7.41	4	-26	26
	Cluster 13	216				
	L Brain Stem		7.06	-6	-36	-48
	Cluster 14	200				
	L Superior Parietal Lobule		6.31	-18	-52	64
	Cluster 15	176				
	L Cingulate Gyrus, posterior division		7.15	-12	-24	40
	Cluster 16	104				
	L Brain Stem		6.27	-8	-28	-18

	Cluster 17	104				
	L Inferior Temporal Gyrus, temporooccipital part		5.82	-44	-60	-12
	Cluster 18	72				
	L Thalamus		5.82	-6	-14	-2
	Cluster 19	40				
	L Brain Stem		6.29	-6	-32	-8
	Cluster 20	40				
	L Lateral Occipital Cortex, superior division		5.70	-30	-82	18
	Cluster 21	24				
	L Brain Stem		5.77	-4	-36	-30
	Cluster 22	24				
	L Middle Frontal Gyrus		5.30	-44	34	36
	Cluster 23	16				
	R Heschls Gyrus (includes H1 and H2)		5.34	46	-14	6
	Cluster 24	16				
	L Inferior Frontal Gyrus, pars opercularis		5.19	-56	12	18
	Cluster 25	16				
	R Cingulate Gyrus, anterior division		5.37	8	38	18
	Cluster 26	16				
	R Lateral Occipital Cortex, superior division		5.22	34	-72	24
	Cluster 27	8				
	L Temporal Pole		5.23	-42	6	-42
	Cluster 28	8				
	L Planum Polare		5.51	-40	-20	-4
	Cluster 29	8				
	R Insular Cortex		5.20	36	-22	6
	Cluster 30	8				
	R Angular Gyrus		5.17	48	-54	56

Supplementary Table S6. Descriptive statistics for clusters and local extrema showing greater activation during the anticipation of Certain Threat relative to Uncertain Threat (FWE $p<0.05$, whole-brain corrected, 4-mm smoothing kernel).

		mm^3	*t*	x	y	z
	Cluster 1	35,560				
	L Precuneus Cortex		11.99	-12	-62	18
	L Lingual Gyrus		11.19	-12	-54	0
	L Cingulate Gyrus, posterior division		8.89	-8	-44	4
	L Hippocampus		7.12	-20	-38	2
	L Thalamus		6.87	-14	-36	4
	R Precuneus Cortex		14.01	14	-58	16
	R Cingulate Gyrus, posterior division		11.01	10	-48	4
	R Cuneal Cortex		10.29	4	-72	28
	R Lateral Occipital Cortex, superior division		10.12	48	-72	34
	R Hippocampus		8.10	18	-36	4
	Cluster 2	21,344				
	L Precentral Gyrus		10.80	-56	-8	46
	L Postcentral Gyrus		9.92	-10	-42	64
	R Postcentral Gyrus		10.73	2	-34	66
	R Precentral Gyrus		8.82	6	-22	66
	Cluster 3	5,208				
	L Lateral Occipital Cortex, superior division		9.77	-38	-80	36
	Cluster 4	4,400				
	R Postcentral Gyrus		9.34	66	-10	30
	R Precentral Gyrus		8.55	60	-6	42
	Cluster 5	2,104				
	L Frontal Medial Cortex		6.63	-4	52	-8
	R Frontal Pole		9.06	0	64	-10
	R Frontal Medial Cortex		7.28	2	50	-12

	Cluster 6	1,904				
	R Hippocampus		11.81	22	-20	-18
	Cluster 7	1,448				
	L Hippocampus		10.29	-22	-20	-16
	L Amygdala		5.86	-12	-6	-20
	Cluster 8	1,168				
	L Central Opercular Cortex		9.57	-38	-12	18
	L Insular Cortex		7.60	-40	-8	6
	Cluster 9	1,048				
	L Parahippocampal Gyrus, posterior division		7.98	-24	-38	-16
	L Temporal Fusiform Cortex, posterior division		7.86	-34	-34	-18
	Cluster 10	856				
	R Lingual Gyrus		9.44	26	-38	-12
	R Parahippocampal Gyrus, posterior division		8.43	26	-34	-16
	R Temporal Fusiform Cortex, posterior division		8.13	34	-36	-14
	Cluster 11	656				
	R Superior Frontal Gyrus		7.01	22	30	44
	Cluster 12	576				
	R Insular Cortex		9.14	38	-8	12
	R Central Opercular Cortex		5.85	46	-10	16
	Cluster 13	536				
	R Middle Temporal Gyrus, anterior division		6.69	60	-4	-16
	Cluster 14	376				
	R Subcallosal Cortex		8.48	2	12	-4
	Cluster 15	272				
	R Lateral Occipital Cortex, superior division		6.03	20	-66	50
	Cluster 16	136				
	L Juxtapositional Lobule Cortex		7.66	-4	0	64
	Cluster 17	120				

	R Postcentral Gyrus		6.09	48	-16	52
	Cluster 18	112				
	L Middle Temporal Gyrus, temporooccipital part		6.07	-60	-62	-8
	L Lateral Occipital Cortex, inferior division		5.57	-58	-68	-8
	Cluster 19	96				
	L Superior Frontal Gyrus		5.67	-22	26	46
	Cluster 20	88				
	L Precuneus Cortex		5.52	-2	-60	64
	Cluster 21	64				
	R Frontal Pole		6.26	0	62	6
	Cluster 22	48				
	R Frontal Pole		5.50	10	70	12
	Cluster 23	48				
	L Lateral Occipital Cortex, superior division		5.76	-8	-86	42
	Cluster 24	40				
	L Lateral Occipital Cortex, superior division		5.42	-16	-84	48
	Cluster 25	32				
	R Accumbens		6.01	12	14	-8
	Cluster 26	32				
	R Caudate		6.12	6	10	-2
	Cluster 27	32				
	R Precuneus Cortex		5.50	12	-50	42
	Cluster 28	24				
	L Middle Temporal Gyrus, anterior division		5.12	-62	-4	-16
	Cluster 29	24				
	L Frontal Pole		5.78	-20	66	12
	Cluster 30	24				
	L Planum Temporale		5.37	-48	-38	16
	Cluster 31	24				

	L Supramarginal Gyrus, posterior division		5.38	-56	-42	18
	Cluster 32	24				
	L Frontal Pole		5.65	-10	70	18
	Cluster 33	24				
	L Superior Parietal Lobule		5.20	-28	-54	52
	Cluster 34	16				
	R Frontal Medial Cortex		5.29	2	40	-18
	Cluster 35	16				
	L Lateral Occipital Cortex, superior division		5.17	-6	-72	58
	Cluster 36	8				
	L Amygdala		5.31	-30	2	-18
	Cluster 37	8				
	R Frontal Pole		5.17	36	38	-8
	Cluster 38	8				
	L Lateral Occipital Cortex, superior division		5.28	-30	-76	48
	Cluster 39	8				
	R Lateral Occipital Cortex, superior division		5.37	20	-64	60

SUPPLEMENTARY REFERENCES

Anderson, J. S., Druzgal, T. J., Lopez-Larson, M., Jeong, E. K., Desai, K., & Yurgelun-Todd, D. (2011). Network anticorrelations, global regression, and phase-shifted soft tissue correction. *Hum Brain Mapp*, *32*(6), 919-934. https://doi.org/10.1002/hbm.21079

Avants, B. B., Tustison, N. J., Song, G., Cook, P. A., Klein, A., & Gee, J. C. (2011). A reproducible evaluation of ANTs similarity metric performance in brain image registration [Article]. *Neuroimage*, *54*, 2033-2044. https://doi.org/10.1016/j.neuroimage.2010.09.025

Avery, S. N., Clauss, J. A., & Blackford, J. U. (2016). The human BNST: Functional role in anxiety and addiction. *Neuropsychopharmacology*, *41*, 126-141. https://doi.org/10.1038/npp.2015.185

Bach, D. R., Castegnetti, G., Korn, C. W., Gerster, S., Melinscak, F., & Moser, T. (2018). Psychophysiological modeling: Current state and future directions. *Psychophysiology*, *55*, e13214. https://doi.org/10.1111/psyp.13209

Bach, D. R., Flandin, G., Friston, K. J., & Dolan, R. J. (2010). Modelling event-related skin conductance responses. *Int J Psychophysiol*, *75*, 349-356. https://doi.org/10.1016/j.ijpsycho.2010.01.005

Bach, D. R., & Friston, K. J. (2013). Model-based analysis of skin conductance responses: Towards causal models in psychophysiology. *Psychophysiology*, *50*, 15-22. https://doi.org/10.1111/j.1469-8986.2012.01483.x

BIAC. (2022). *IXI Dataset*. Imperial College London. Retrieved April 19 from https://brain-development.org/ixi-dataset/

Bo, K., Kraynak, T. E., Kwon, M., Sun, M., Gianaros, P. J., & Wager, T. D. (2024). A systems identification approach using Bayes factors to deconstruct the brain bases of emotion regulation. *Nat Neurosci*, *27*, 975-987. https://doi.org/10.1038/s41593-024-01605-7

Cohen, J. (1988). *Statistical power analysis for the behavioral sciences* (2nd ed.). Lawrence Erlbaum Associates.

Cohen, J. R. (1994). The earth is round (p < .05). *American Psychologist*, *49*, 997-1003. https://doi.org/10.1037/0003-066X.49.12.997

Cornwell, B. R., Didier, P. R., Grogans, S. E., Anderson, A. S., Islam, S., Kim, H. C., . . . Shackman, A. J. (2025). A shared threat-anticipation circuit is dynamically engaged at different moments by certain and uncertain threat. *Journal of Neuroscience*, *45*, e2113242025. https://doi.org/10.1523/JNEUROSCI.2113-24.2025

Cox, R. W. (1996). AFNI: Software for analysis and visualization of functional magnetic resonance neuroimages. *Computers and Biomedical Research*, *29*, 162-173.

Daldrup, T., Remmes, J., Lesting, J., Gaburro, S., Fendt, M., Meuth, P., . . . Seidenbecher, T. (2015). Expression of freezing and fear-potentiated startle during sustained fear in mice. *Genes Brain Behav*, *14*, 281-291. https://doi.org/10.1111/gbb.12211

Daniel-Watanabe, L., & Fletcher, P. C. (2022). Are fear and anxiety truly distinct? *Biological Psychiatry Global Open Science*, *2*, 341-349. https://doi.org/https://doi.org/10.1016/j.bpsgos.2021.09.006

Davis, M., Walker, D. L., Miles, L., & Grillon, C. (2010). Phasic vs sustained fear in rats and humans: Role of the extended amygdala in fear vs anxiety. *Neuropsychopharmacology*, *35*, 105-135. https://doi.org/10.1038/npp.2009.109

Desikan, R. S., Ségonne, F., Fischl, B., Quinn, B. T., Dickerson, B. C., Blacker, D., . . . Killiany, R. J. (2006). An automated labeling system for subdividing the human cerebral cortex on MRI scans into gyral based regions of interest. *Neuroimage*, *31*, 968-980.

Domschke, K. (2022). Fear and anxiety-Distinct or "kindred" phenomena? *Biol Psychiatry Glob Open Sci*, *2*, 314-315. https://doi.org/10.1016/j.bpsgos.2022.07.001

Edlow, B. L., Takahashi, E., Wu, O., Benner, T., Dai, G., Bu, L., . . . Folkerth, R. D. (2012). Neuroanatomic connectivity of the human ascending arousal system critical to consciousness and its disorders. *J Neuropathol Exp Neurol*, *71*(6), 531-546. https://doi.org/10.1097/NEN.0b013e3182588293

Eskildsen, S. F., Coupé, P., Fonov, V., Manjón, J. V., Leung, K. K., Guizard, N., . . . Alzheimer's Disease Neuroimaging Initiative. (2012). BEaST: brain extraction based on nonlocal segmentation technique. *Neuroimage*, *59*, 2362-2373.

Fox, A. S., Lapate, R. C., Davidson, R. J., & Shackman, A. J. (2018). The nature of emotion: A research agenda for the 21st century. In A. S. Fox, R. C. Lapate, A. J. Shackman, & R. J. Davidson (Eds.), *The nature of emotion. Fundamental questions* (2nd ed., pp. 403-417). Oxford University Press.

Fox, A. S., & Shackman, A. J. (2019). The central extended amygdala in fear and anxiety: Closing the gap between mechanistic and neuroimaging research. *Neuroscience letters*, *693*, 58-67. https://doi.org/https://doi.org/10.1016/j.neulet.2017.11.056

Frazier, J. A., Chiu, S., Breeze, J. L., Makris, N., Lange, N., Kennedy, D. N., . . . Biederman, J. (2005). Structural brain magnetic resonance imaging of limbic and thalamic volumes in pediatric bipolar disorder. *American Journal of Psychiatry*, *162*, 1256-1265.

Grabner, G., Janke, A. L., Budge, M. M., Smith, D., Pruessner, J., & Collins, D. L. (2006). Symmetric atlasing and model based segmentation: an application to the hippocampus in older adults. *Med Image Comput Comput Assist Interv Int Conf Med Image Comput Comput Assist Interv*, *9*, 58–66. https://doi.org/https://doi.org/10.1007/11866763_8

Grogans, S. E., Bliss-Moreau, E., Buss, K. A., Clark, L. A., Fox, A. S., Keltner, D., . . . Shackman, A. J. (2023). The nature and neurobiology of fear and anxiety: State of the science and opportunities for accelerating discovery. *Neuroscience & Biobehavioral Reviews*, *151*, 105237. https://doi.org/https://doi.org/10.1016/j.neubiorev.2023.105237

Grogans, S. E., Hur, J., Barstead, M. G., Anderson, A. S., Islam, S., Kuhn, M., . . . Shackman, A. J. (2024). Neuroticism/negative emotionality is associated with increased reactivity to uncertain threat in the bed nucleus of the stria terminalis, not the amygdala. *Journal of Neuroscience*, *44*, e1868232024.

Gronau, Q. F., Ly, A., & Wagenmakers, E.-J. (2020). Informed Bayesian t-Tests. *The American Statistician*, *74*, 137-143. https://doi.org/10.1080/00031305.2018.1562983

Grupe, D. W., & Nitschke, J. B. (2013). Uncertainty and anticipation in anxiety: an integrated neurobiological and psychological perspective. *Nat Rev Neurosci*, *14*, 488-501. https://doi.org/nrn3524 [pii]

10.1038/nrn3524

Gungor, N. Z., & Paré, D. (2016). Functional heterogeneity in the bed nucleus of the stria terminalis. *Journal of Neuroscience*, *36*, 8038-8049.

Hefner, K. R., Moberg, C. A., Hachiya, L. Y., & Curtin, J. J. (2013). Alcohol stress response dampening during imminent versus distal, uncertain threat. *J Abnorm Psychol*, *122*, 756-769. https://doi.org/10.1037/a0033407

Henson, R. (2007). Efficient experimental design for fMRI. In K. Friston, J. Ashburner, S. Kiebel, T. Nichols, & W. Penny (Eds.), *Statistical Parametric Mapping: The Analysis of Functional Brain Images* (pp. 193-210). Academic Press.

Hur, J., Smith, J. F., DeYoung, K. A., Anderson, A. S., Kuang, J., Kim, H. C., . . . Shackman, A. J. (2020). Anxiety and the neurobiology of temporally uncertain threat anticipation. *Journal of Neuroscience*, *40*, 7949-7964. https://doi.org/10.1101/2020.02.25.964734

Jenkinson, M., Beckmann, C. F., Behrens, T. E., Woolrich, M. W., & Smith, S. M. (2012). FSL. *Neuroimage*, *62*, 782-790. https://doi.org/10.1016/j.neuroimage.2011.09.015

Kim, H. C., Kaplan, C. M., Islam, S., Anderson, A. S., Piper, M. E., Bradford, D. E., . . . Shackman, A. J. (2023). Acute nicotine abstinence amplifies subjective withdrawal symptoms and threat-evoked fear and anxiety, but not extended amygdala reactivity. *PLoS One*, *18*, e0288544. https://doi.org/https://doi.org/10.1371/journal.pone.0288544

Kruger, O., Shiozawa, T., Kreifelts, B., Scheffler, K., & Ethofer, T. (2015). Three distinct fiber pathways of the bed nucleus of the stria terminalis to the amygdala and prefrontal cortex. *Cortex*, *66*, 60-68. https://doi.org/10.1016/j.cortex.2015.02.007

Lange, M. D., Daldrup, T., Remmers, F., Szkudlarek, H. J., Lesting, J., Guggenhuber, S., . . . Pape, H. C. (2017). Cannabinoid CB1 receptors in distinct circuits of the extended amygdala determine fear responsiveness to unpredictable threat. *Mol Psychiatry*, *22*, 1422-1430. https://doi.org/10.1038/mp.2016.156

Lebow, M. A., & Chen, A. (2016). Overshadowed by the amygdala: the bed nucleus of the stria terminalis emerges as key to psychiatric disorders. *Mol Psychiatry*, *21*, 450-463. https://doi.org/10.1038/mp.2016.1

LeDoux, J. E., & Pine, D. S. (2016). Using neuroscience to help understand fear and anxiety: A two-system framework. *Am J Psychiatry*, *173*, 1083-1093. https://doi.org/10.1176/appi.ajp.2016.16030353

Lorio, S., Fresard, S., Adaszewski, S., Kherif, F., Chowdhury, R., Frackowiak, R. S., . . . Draganski, B. (2016). New tissue priors for improved automated classification of subcortical brain structures on MRI. *Neuroimage*, *130*, 157-166. https://doi.org/10.1016/j.neuroimage.2016.01.062

Love, J., Selker, R., Marsman, M., Jamil, T., Dropmann, D., Verhagen, J., . . . Wagenmakers, E.-J. (2019). JASP: Graphical statistical software for common statistical designs. *Journal of Statistical Software*, *88*, 1-17. https://doi.org/10.18637/jss.v088.i02

Makris, N., Goldstein, J. M., Kennedy, D., Hodge, S. M., Caviness, V. S., Faraone, S. V., . . . Seidman, L. J. (2006). Decreased volume of left and total anterior insular lobule in schizophrenia. *Schizophrenia Research*, *83*, 155-171.

McCormick, M., Liu, X., Jomier, J., Marion, C., & Ibanez, L. (2014). ITK: enabling reproducible research and open science. *Frontiers in Neuroinformatics*, *8*, 13. https://doi.org/10.3389/fninf.2014.00013

Miles, L., Davis, M., & Walker, D. (2011). Phasic and sustained fear are pharmacologically dissociable in rats. *Neuropsychopharmacology*, *36*, 1563-1574. https://doi.org/10.1038/npp.2011.29

Mobbs, D., Headley, D. B., Ding, W., & Dayan, P. (2020). Space, time, and fear: Survival computations along defensive circuits. *Trends in cognitive sciences*, *24*, 228-241. https://doi.org/10.1016/j.tics.2019.12.016

Moberg, C. A., Bradford, D. E., Kaye, J. T., & Curtin, J. J. (2017). Increased startle potentiation to unpredictable stressors in alcohol dependence: Possible stress neuroadaptation in humans. *Journal of Abnormal Psychology*, *126*, 441-453. https://doi.org/10.1037/abn0000265

Moscarello, J. M., & Penzo, M. A. (2022). The central nucleus of the amygdala and the construction of defensive modes across the threat-imminence continuum. *Nat Neurosci*, *25*, 999-1008. https://doi.org/10.1038/s41593-022-01130-5

Nichols, T., Brett, M., Andersson, J., Wager, T., & Poline, J. B. (2005). Valid conjunction inference with the minimum statistic. *Neuroimage*, *25*, 653-660. https://doi.org/S1053-8119(04)00750-5 [pii]

10.1016/j.neuroimage.2004.12.005 [doi]

NIMH. (2011). *Negative valence systems: Workshop proceedings (March 13, 2011 – March 15, 2011; Rockville, Maryland)*. Retrieved July 1 from https://www.nimh.nih.gov/research/research-funded-by-nimh/rdoc/negative-valence-systems-workshop-proceedings.shtml

Orederu, T., Lennon, V., Vervliet, B., & Schiller, D. (2024). Fear. In A. Scarantino (Ed.), *Emotion Theory* (Vol. II, pp. 152-175). Routledge.

Perusini, J. N., & Fanselow, M. S. (2015). Neurobehavioral perspectives on the distinction between fear and anxiety. *Learn Mem*, *22*, 417-425. https://doi.org/10.1101/lm.039180.115

Poldrack, R. A., Baker, C. I., Durnez, J., Gorgolewski, K. J., Matthews, P. M., Munafo, M. R., . . . Yarkoni, T. (2017). Scanning the horizon: towards transparent and reproducible neuroimaging research. *Nat Rev Neurosci*, *18*, 115-126. https://doi.org/10.1038/nrn.2016.167

Pruim, R. H. R., Mennes, M., van Rooij, D., Llera, A., Buitelaar, J. K., & Beckmann, C. F. (2015). ICA-AROMA: a robust ICA-based strategy for removing motion artifacts from fMRI data. *Neuroimage*, *112*, 267-277.

Rorden, C. (2019, September 2, 2019). *MRIcron*. NITRC. Retrieved April 18 from https://www.nitrc.org/projects/mricron

Schimmack, U. (2019). *Statistics wars: Don't change alpha. Change the null-hypothesis!* Retrieved December 15 from https://replicationindex.com/category/nil-hypothesis/

Schmalz, X., Biurrun Manresa, J., & Zhang, L. (2023). What is a Bayes factor? *Psychological Methods*, *28*, 705-718. https://doi.org/10.1037/met0000421

Schönbrodt, F. D., Wagenmakers, E. J., Zehetleitner, M., & Perugini, M. (2017). Sequential hypothesis testing with Bayes factors: Efficiently testing mean differences. *Psychol Methods*, *22*, 322-339. https://doi.org/10.1037/met0000061

Shackman, A. J., & Fox, A. S. (2016). Contributions of the central extended amygdala to fear and anxiety. *Journal of Neuroscience*, *36*, 8050-8063. https://doi.org/10.1523/JNEUROSCI.0982-16.2016

Shackman, A. J., Tromp, D. P. M., Stockbridge, M. D., Kaplan, C. M., Tillman, R. M., & Fox, A. S. (2016). Dispositional negativity: An integrative psychological and neurobiological perspective. *Psychological Bulletin*, *142*, 1275-1314.

ten Donkelaar, H. J., Tzourio-Mazoyer, N., & Mai, J. K. (2018). Toward a common terminology for the gyri and sulci of the human cerebral cortex [Review]. *Frontiers in Neuroanatomy*, *12*, 93. https://doi.org/10.3389/fnana.2018.00093

Theiss, J. D., Ridgewell, C., McHugo, M., Heckers, S., & Blackford, J. U. (2017). Manual segmentation of the human bed nucleus of the stria terminalis using 3T MRI. *Neuroimage*, *146*, 288-292. https://doi.org/10.1016/j.neuroimage.2016.11.047

Tillman, R. M., Stockbridge, M. D., Nacewicz, B. M., Torrisi, S., Fox, A. S., Smith, J. F., & Shackman, A. J. (2018). Intrinsic functional connectivity of the central extended amygdala. *Human Brain Mapping*, *39*, 1291-1312.

Tovote, P., Fadok, J. P., & Lüthi, A. (2015). Neuronal circuits for fear and anxiety. *Nat Rev Neurosci*, *16*, 317-331. https://doi.org/10.1038/nrn3945

Tukey, J. W. (1977). *Exploratory data analysis*. Addison Wesley.

Tustison, N. J., Avants, B. B., Cook, P. A., Zheng, Y. J., Egan, A., Yushkevich, P. A., & Gee, J. C. (2010). N4ITK: Improved N3 bias correction [Article]. *IEEE Transactions on Medical Imaging*, *29*, 1310-1320. https://doi.org/10.1109/tmi.2010.2046908

van Doorn, J., van den Bergh, D., Böhm, U., Dablander, F., Derks, K., Draws, T., . . . Wagenmakers, E.-J. (2021). The JASP guidelines for conducting and reporting a Bayesian analysis. *Psychonomic Bulletin & Review*, *28*, 813-826. https://doi.org/10.3758/s13423-020-01798-5

Wagenmakers, E.-J., Love, J., Marsman, M., Jamil, T., Ly, A., Verhagen, J., . . . Morey, R. D. (2018). Bayesian inference for psychology. Part II: Example applications with JASP. *Psychonomic Bulletin & Review*, *25*, 58-76. https://doi.org/10.3758/s13423-017-1323-7

Walter, A., Mai, J., Lanta, L., & Görcs, T. (1991). Differential distribution of immunohistochemical markers in the bed nucleus of the stria terminalis in the human brain. *J Chem Neuroanat*, *4*(4), 281-298.

Wellcome Centre for Human Neuroimaging. (2022). *SPM*. University College London. Retrieved April 18 from https://fil.ion.ucl.ac.uk/spm/

Wickham, H. (2016). *ggplot2: Elegant graphics for data analysis* (2nd ed.). Springer-Verlag.